INTERNATIONAL JOURNAL OF CLIMATOLOGY
Int. J. Climatol. (2011)
Published online in Wiley Online Library
(wileyonlinelibrary.com) DOI: 10.1002/joc.2421

The future of dry and wet spells in Europe: A comprehensive study based on the ENSEMBLES regional climate models

Georg Heinrich* and Andreas Gobiet

Wegener Center for Climate and Global Change (WEGC) and Institute for Geophysics, Astrophysics, and Meteorology/Institute of Physics (IGAM/IP), University of Graz, Graz, Austria

ABSTRACT: Under the aspect of future climate change, it is important for decision makers to know how drought conditions might change on the regional scale in order to map out adequate adaptation and mitigation strategies. Recent RCM simulations provided by the ENSEMBLES project are used to analyse changes in dry and wet conditions in Europe by the mid of the 21st century under the A1B emission scenario. Eight RCMs are selected to capture the uncertainties of the projected changes. An empirical statistical error correction approach is applied to modelled daily mean air temperature and precipitation amount to account for RCM errors, and commonly used drought indices – the Standardized Precipitation Index (SPI), the self calibrated Palmer Z-Index (scZI) and Palmer Drought Severity Index (scPDSI) – are calculated. Changes in the mean, in interannual variability, and in frequency, length, distance, magnitude, and area of dry and wet events are investigated. The statistical significance of the projected multi-model mean changes and the according uncertainties are analysed for nine European subregions. Furthermore, distributional changes of the dry and wet spell characteristics are assessed. Changes in the mean, and in dry and wet event characteristics show the most pronounced changes towards drier and wetter conditions in the southern- and northernmost European subregions, respectively. Here, the changes are highly significant and confident, while the projected changes are more dissonant for the other subregions. Severe changes in the extremes of event length, distance, magnitude, and area particularly arise in the southern- and northernmost European subregions. The projected changes in interannual variability are less significant and confident. However, significantly increasing interannual variability is projected in regions with pronounced changes in the mean towards wetter as well as towards drier conditions. Copyright © 2011 Royal Meteorological Society

KEY WORDS climate change; drought; Europe; Regional Climate Models; ENSEMBLES; uncertainty; Standardized Precipitation Index; self-calibrated Palmer Drought Severity Index

Received 19 August 2010; Revised 5 May 2011; Accepted 27 July 2011

1. Introduction

Drought is a natural recurrent phenomenon which occurs on a variety of different temporal and spatial scales and significantly affects natural and socio-economic systems. Nowadays, much effort is made to monitor and forecast drought events in order to be able to intervene and mitigate drought impacts (e.g. Drought Management Centre for Southeastern Europe (DMCSEE); European Drought Centre (EDC); U.S. National Drought Mitigation Center (NDMC)). Furthermore, it is important for decision makers to know how drought conditions might change in future, in order to map out adequate adaptation and mitigation strategies.

The definition of drought is highly varied because of its strong dependency on time and space and its variety of impacts. However, the widely accepted classification of drought is: (1) Meteorological drought; (2) agricultural drought; (3) hydrological drought; and (4) socio-economic drought (Wilhite and Glantz, 1985; Hayes *et al*., 2010). Meteorological drought is associated with a precipitation shortage. Dependent upon its duration, meteorological drought can result in agricultural (related to soil moisture) or hydrological drought (related to e.g. stream flow, ground water level, reservoir storage). Socio-economic drought addresses the monetary effects of drought. Among the variety of existing drought indices, the Standardized Precipitation Index (SPI; McKee *et al*., 1993) and the Palmer Drought Severity Index (PDSI; Palmer, 1965) are well known and widely used (Heim, 2002; Keyantash and Dracup, 2002; Hayes *et al*., 2010). The SPI is based solely on precipitation, while the PDSI additionally accounts for air temperature via potential evapotranspiration.

Many studies investigated drought conditions of the past using the SPI and/or the PDSI and found evidence of increasing drought risk in central, eastern, and southern Europe during the last century (e.g. Szinell *et al*., 1998; Lloyd-Hughes and Saunders, 2002; Bonaccorso *et al*., 2003; Dai *et al*., 2004; Trnka *et al*., 2008; Briffa *et al*., 2009). Future drought projections can be derived from physical-based general circulation models (GCMs) making assumptions about the future socio-economic

* Correspondence to: Georg Heinrich, Wegener Zentrum für Klima und Globalen Wandel, Karl-Franzens-Universität Graz, Leechgasse 25, A-8010 Graz. E-mail: g.heinrich@uni-graz.at

Copyright © 2011 Royal Meteorological Society

development and the associated greenhouse gas (GHG) emissions. Uncertainties in future climate projections arise from the choice of the GHG emission scenario, GCM internal uncertainty (initial condition uncertainty), and model formulation uncertainty (Collins, 2007). In order to give a reliable assessment of future drought conditions, these uncertainties have to be taken into account. Therefore, an ensemble of different model projections is commonly used which consists of multiple realisations from one model and/or multi-model projections. For example, Giorgi (2006) used a set of 20 GCMs and calculated a climate index based on changes in the mean and in interannual variability of air temperature and precipitation for 26 land regions worldwide. He detected the Mediterranean and northeastern parts of Europe as most responsive regions to climate change by the end of the 21st century. The high vulnerability of southern European regions to future drought regimes was underlined by various other studies. For example, Burke and Brown (2008) calculated the SPI and PDSI based on a large ensemble of GCMs and found that the PDSI shows a higher increase in the proportion of the global land surface in drought than the SPI for a double CO_2 climate. The most consistent increase in drought was detected in regions where annual precipitation decreases as in the Mediterranean region. Sheffield and Wood (2008) analysed future changes in soil moisture using eight GCMs and showed that besides an increase in the spatial extent of drought, drought frequencies are likely to increase by the end of the 21st century for the Mediterranean region. Warren *et al*. (2009) calculated the SPI using four GCMs and concluded robust increases in drought in Europe during the 21st century. Lehner *et al*. (2006) investigated the impact of global climate change on hydrological drought using two GCMs and found that northern and northeastern Europe are most prone to a rise in flood frequencies, while southern and southeastern Europe show significant increases in drought frequencies.

Current GCMs have a fairly coarse horizontal resolution (100–200 km grid spacing) and, therefore, are unable to reproduce small-scale climate characteristics such as orographic precipitation (e.g. McGregor, 1997). In order to conduct climate simulations with a finer horizontal resolution, which make it possible to resolve physical processes at smaller scales, regional climate models (RCMs) are nested within the GCM large-scale atmospheric circulation over a limited area (e.g. Giorgi and Mearns, 1991, 1999; McGregor, 1997; Wang *et al*., 2004). Drought can be considered a regional phenomenon (e.g. Wilhite, 1993) and its variability is likely to increase as one moves towards more localized scales. Therefore, it can be expected that the use of RCMs improves the regional representation of drought events as they have the potential to better represent local climate variability and extremes (Rummukainen, 2010). Although some studies demonstrated a tendency towards drier (wetter) conditions in southern (northern) Europe using RCMs (e.g. Beniston *et al*., 2007; Blenkinsop and Fowler 2007, López-Moreno and Beniston, 2009), according to the authors' knowledge no comprehensive RCM-based study exists so far which analyses changes of dry and wet conditions for all of Europe by means of commonly used drought indices.

The objective of this study is to provide comprehensive information on how dry and wet spell characteristics might change by the mid of the 21st century in Europe. For this purpose, we investigate and compare multiple commonly used drought indices and drought characteristics. The SPI is calculated in order to analyse projected precipitation changes of various time scales. Since the SPI does not account for future changes in air temperature, we complement this study by computing the self-calibrated Palmer Z-Index (scZI) and PDSI (scPDSI). The uncertainties associated with these projections are regarded by analysing an ensemble of the newest available RCM simulations from the EU-FP6 integrated project ENSEMBLES (http://ensembles-eu.org).

The content of this paper is structured as follows. Section 2 introduces the data and the study region. Section 3 describes the drought indices which are analysed with respect to their changes in the mean, in interannual variability, and in dry and wet event characteristics in Section 4. Section 5 summarizes the key findings of this study.

2. Data

2.1. RCM selection

In the ENSEMBLES project, a set of 20 high-resolution RCM simulations with a horizontal grid spacing of about 25 km and driven by 8 different GCMs was produced (as at May 2010). Owing to limited computational resources not all GCM-RCM combinations could be realized. The subsampling mainly addressed uncertainty in boundary conditions (choice of GCM) and RCM model formulation (van der Linden and Mitchell, 2009). Since the choice of the GHG emission scenario is less important till the mid of the 21st century (Prein *et al*., (unpublished)), only the A1B emission scenario (Nakicenovic *et al*., 2000) was used to force the climate simulations.

Déqué *et al*. (2007, 2011) showed that both the choice of the GCM and RCM are major sources of uncertainty. To avoid under-sampling of uncertainty when using a subset of the available RCM simulations produced within ENSEMBLES, it is proposed to use at least two or more RCMs that are forced by at least two GCMs (van der Linden and Mitchell, 2009). For this study, a subset of eight RCM simulations driven by five different GCMs is selected (Table I). Until now, most studies have randomly selected a subset of RCM or GCM simulations from the entire ensemble. This potentially leads to sampling errors and, therefore, to the risk of introducing systematic over- or underestimation of uncertainty. To avoid this problem, the RCM selection in this study is based on seasonal climate change signals for air temperature (2 m above ground) and precipitation amount between the periods of 1961–1990 and 2021–2050 over Europe. For this purpose, only simulations which cover all of

Copyright © 2011 Royal Meteorological Society

Table I. RCM simulations used in this study.

Model No.	Institute	RCM	Driving GCM	Acronym	Simulation period
1	C4I	RCA3	HadCM3Q16	C4IRCA3	1951–2099
2	CNRM	ALADIN	ARPEGE	CNRM-RM4.5	1951–2050
3	ETHZ	CLM	HadCM3Q0	ETHZ-CLM	1951–2099
4	HC	HadRM3Q16	HadCM3Q16	METO-HC_HadRM3Q16	1951–2100
5	ICTP	RegCM	ECHAM5-r3	ICTP-REGCM3	1951–2100
6	KNMI	RACMO	ECHAM5-r3	KNMI-RACMO2	1950–2100
7	SMHI	RCA	BCM	SMHIRCA	1961–2100
8	UCLM	PROMES	HadCM3Q0	UCLM-PROMES	1951–2050

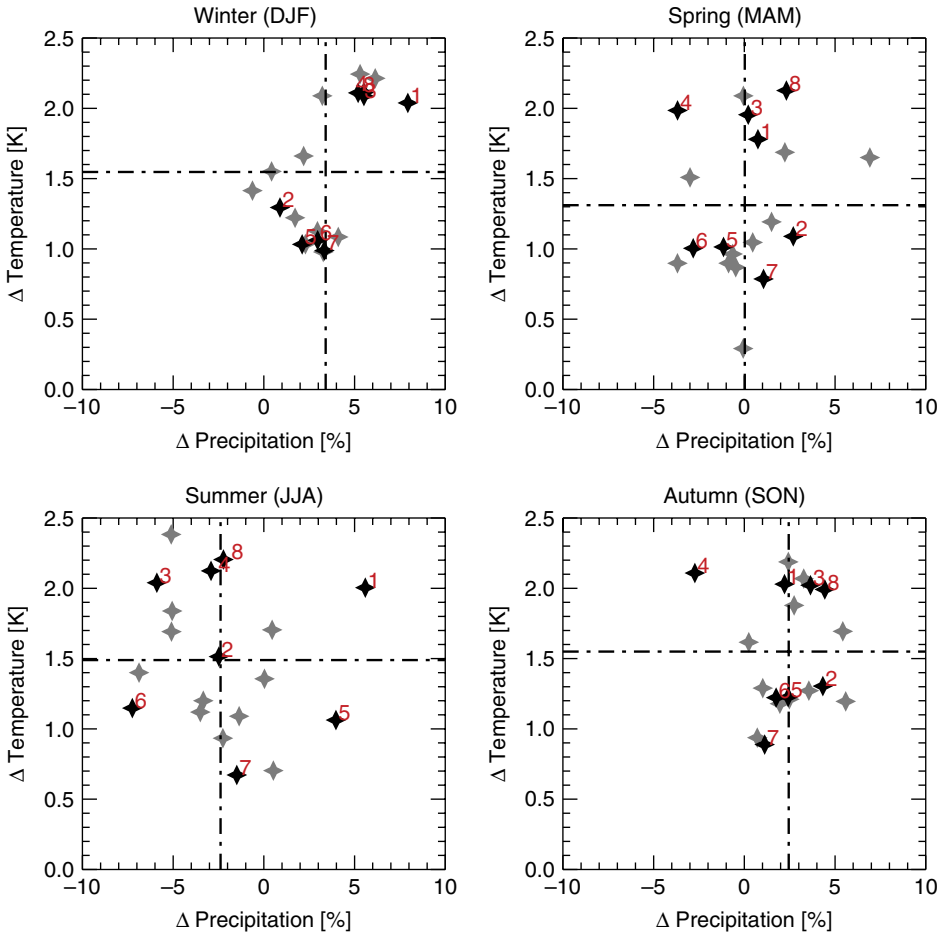

Figure 1. Scatter diagrams of the projected seasonal mean changes between 1961 and 1990, and 2021 and 2050 in air temperature and precipitation over Europe for the ENSEMBLES regional climate models (as at May 2010). Precipitation changes are relative with respect to the baseline period. Dashed lines display the multi-model mean changes, and black shaded symbols labelled with numbers indicate the selected models (ref. Table I). This figure is available in colour online at wileyonlinelibrary.com/journal/joc

Europe are analysed (19 simulations). The basic idea was to choose two models of each quadrant spanned by the multi-model averages of air temperature and precipitation, in order to appropriately represent the point cloud of Figure 1. Therefore, four cases are considered comprising warmer/drier, warmer/wetter, colder/drier, and colder/wetter conditions, than the ensemble mean of all 19 simulations.

From Figure 1 it can be seen that the two models ETHZ-CLM (model no. 3) and METO-HC_HadCM3Q16 (model no. 4) show higher air temperature and lower precipitation changes than the multi-model mean in summer and spring. On the contrary, C4IRCA3 (model no. 1) and UCLM-PROMES (model no. 8) exhibit higher air temperature and precipitation changes. The two models KNMI-RACMO2 (model no. 6) and CNRM-RM4.5 (model no. 2) are selected to cover the case of colder/drier conditions, and on the other hand, ICTP-REGCM3 (model no. 5) and SMHIRCA (model no. 7) are selected to represent colder/wetter conditions than the multi-model mean.

Copyright © 2011 Royal Meteorological Society

2.2. Observational data and RCM error correction

Although RCMs have considerable advantage over GCMs in reproducing regional climate features, they are also known to feature substantial model errors (e.g. Frei *et al*., 2003; Hagemann *et al*., 2004; Suklitsch *et al*., 2008, 2010 (in Press)) which affect the assessment of climate change impacts. In order to correct the error characteristics of the RCM simulations, a quantile-based error-correction approach (Quantile Mapping; QM) is applied on a daily basis to mean air temperature and precipitation amount for each of the eight RCMs separately (e.g. Dobler and Ahrens, 2008; Piani *et al*., 2009). The error correction method is selected according to Themeßl *et al*. 2011, who showed the superior performance of QM compared to six other error correction approaches for daily precipitation over the Alpine region. QM aims at adjusting the empirical cumulative distribution functions (ECDFs) of modelled to observed data and, therefore, accounts for errors in the shape of the modelled distribution under the assumption that the observed data is free of errors. For this study, QM is based on daily and point-wise derived ECDFs of the baseline period and the RCM output is bilinearly interpolated to the grid of the observational dataset. For each day of the year a 31-day moving window, centred at the focus day, is used for construction of the ECDFs. In contrast to Themeßl *et al*. 2011, who used the reanalysis-driven hindcast simulation, here QM is based on the ECDF of the GCM-driven control simulation and, therefore, accounts for the combined GCM-RCM error. Furthermore, the method is not restricted to historical extremes of the baseline period since the actual model value is corrected by the difference between modelled and observed value of the corresponding quantile instead of pure empirical mapping.

The observational basis for the error correction is the 0.22° rotated version of the gridded E-OBS-v1.0 dataset (E-OBS). E-OBS comprises daily gridded mean, minimum, and maximum surface air temperature and precipitation amount for entire Europe on four spatial resolutions covering the period of 1950–2006 (Haylock *et al*., 2008). Hofstra *et al*. (2009) analysed the error characteristics of E-OBS compared to other gridded datasets which have been developed with much higher station density for smaller parts of Europe. They found a negative bias for precipitation and a slight positive bias for air temperature, whereas the correlation is excellent. Apart from the fact that E-OBS provides the first high-resolution gridded dataset product of daily climate over Europe, the usage of E-OBS within this study has two additional advantages: (1) It provides best estimates of grid-box averages rather than point values and, therefore, allows direct comparison with RCM output; and (2) The grid of the 0.22° rotated version of the E-OBS dataset is defined according to the grids of the RCMs and, therefore, interpolation errors are potentially reduced.

2.3. Study regions

The focus of this study is on nine European subregions displayed in Figure 2, according to the studies

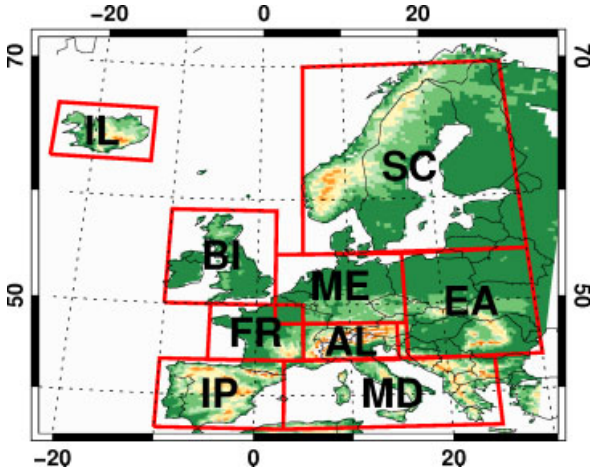

Figure 2. The nine subregions studied: Iberian Peninsula (IP), Mediterranean (MD), France (FR), Middle Europe (ME), Alps (AL), Eastern Europe (EA), British Isles (BI), Iceland (IL), and Scandinavia (SC). This figure is available in colour online at wileyonlinelibrary.com/journal/joc

conducted within PRUDENCE (http://prudence.dmi.dk/) and ENSEMBLES (Christensen and Christensen, 2007). Figure 3 depicts the subregional mean annual cycle of air temperature and precipitation in the baseline period, showing the observations, as well as the range of the error-corrected RCM results. The graphical representation follows the climate diagram system of Walter and Lieth (Walter and Lieth, 1967), which indicates arid (humid) months if the air temperature line is above (beneath) the precipitation line. First, it can be seen that the error correction method performs well in adjusting the simulated monthly mean values to the observational data. The eight RCMs indicate deviations from the observed climatological monthly mean values ranging from −12.0% to +10.9% for precipitation. Air temperature indicates a range between −0.5 K and +0.9 K, and thus the deviations are not visible in Figure 3 due to the scale of the ordinate. Second, Figure 3 highlights the diversity of subregional climate characteristics in Europe which are mainly dependent upon latitude, distance from sea, and local influences such as orography. The southern European regions (Iberian Peninsula (IP) and Mediterranean (MD)) show arid climate features during summer. France (FR) and Middle Europe (ME) mark the transition from maritime towards continental climate. Eastern Europe (EA) shows a highly pronounced humid continental climate with large differences between summer and winter air temperature and a maximum of precipitation amount during summer. The Alpine region (AL) is locally influenced by the Alpine crest and exhibits a pronounced humid climate with high precipitation amounts over the entire year. The northern subregions (British Isles (BI) and Iceland (IL)) have humid maritime climate characteristics with a precipitation minimum (maximum) in summer (winter) and relatively low annual variability of air temperature. Scandinavia (SC) has both maritime and continental influences, and for the subregional mean,

Copyright © 2011 Royal Meteorological Society

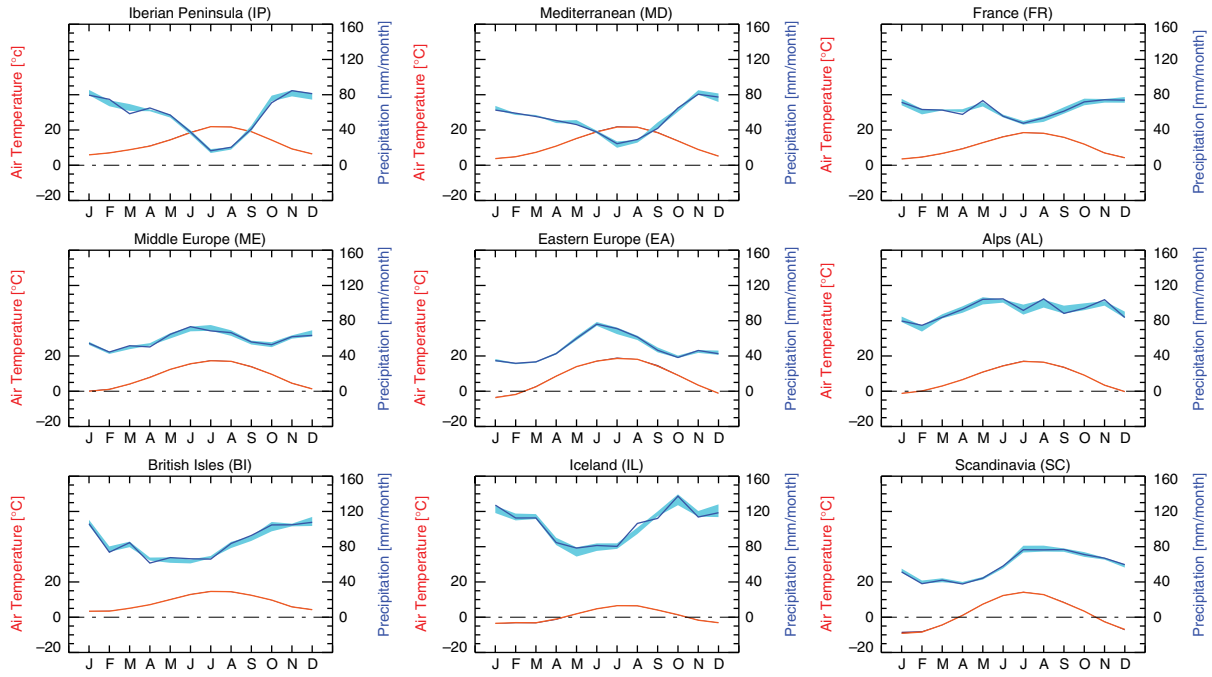

Figure 3. Walter–Lieth climate diagrams of the nine subregions for the baseline period. The solid line depicts the regional mean of the observational E-OBS dataset and the shaded areas represent the range of the error corrected RCMs. Red and blue colours display air temperature and precipitation, respectively. This figure is available in colour online at wileyonlinelibrary.com/journal/joc

a humid climate with low winter air temperature and less precipitation in the first half of the year is observed.

2.4. Soil data

The calculation of the scPDSI requires the knowledge of potential soil moisture storage capacity. This data has been obtained from the Food and Agriculture Organization (FAO) digital soil map of the world (FAO, 2003) which is commonly used for the calculation of the PDSI (e.g. van der Schrier *et al*., 2007; Briffa *et al*., 2009). The dataset has a horizontal resolution of 5′ and comprises for each grid cell the dominant (60%) and associated (40%) water holding capacity (WHC) of 9 classes. For further use, the weighted mean of the two different classes for each grid cell is calculated, and no WHC is attributed if the dominant WHC is not available. The data is then bilinearly interpolated to the common E-OBS grid.

3. Methods

3.1. Calculation of the Standardized Precipitation Index

McKee *et al*. (1993) introduced the SPI as a versatile tool in drought monitoring and analysis which only requires precipitation as input and can be calculated for a variety of time scales. Short-term SPIs showed their ability for monitoring agricultural droughts (e.g. Ji and Peters, 2003; Labedzki, 2007), while longer-term SPIs indicate hydrological drought events (e.g. Bussay *et al*., 1999; Szalai and Szinell, 2000; Seiler *et al*., 2002).

In the first step of the monthly SPI calculation procedure for different time scales i, the precipitation amount of the actual and the preceding i-1 months is summed up as a running total (PRi). In a second step, the parameters of the two-parameter Gamma distribution are estimated for the precipitation amounts of each of the 12 months of a year using maximum-likelihood approximations (e.g. Lloyd-Hughes and Saunders, 2002; Wu *et al*., 2005; Dubrovsky *et al*., 2008). The estimated distribution parameters are then used to calculate the monthly SPIi following

$$SPIi = f^{-1}(g(\mathrm{PRi})), \tag{1}$$

where g denotes the cumulative probability of the Gamma distribution for PRi and f^{-1} is the inverse cumulative standard normal distribution which is approximated following Abramowitz and Stegun (1965). According to Equation (1), each monthly PRi is transformed to a value of the standard normal distribution and, therefore, represents the deviation from the mean in units of standard deviations. The SPIs analysed in this study are calculated by averaging the monthly SPIs over the corresponding months. For example, the SPI3 for the winter season (DJF) is computed as the mean of the monthly SPI3 over December, January, and February.

The main advantages of the SPI are its clarity and flexibility. Disadvantages encompass the need of long time series and, as applied here, the assumption that the Gamma distribution properly describes the data (Hayes *et al*., 1999). McKee *et al*. (1993) suggest using a continuous period of at least 30 years to fit the distribution. The SPI was originally designed to express drought severity with respect to a given location and period. Since the SPI is a normalized measure relative to a specific location and

Copyright © 2011 Royal Meteorological Society

Table II. Classification of the SPI.

SPI	Class
≥2.00	Extremely wet
1.50 to 1.99	Very wet
1.00 to 1.49	Moderately wet
−0.99 to 0.99	Near normal
−1.00 to −1.49	Moderately dry
−1.50 to −1.99	Severely dry
≤−2.00	Extremely Dry

period, the frequency of different SPI-classes (Table II) is climatologically consistent for any site. Therefore, it is not possible to use the original SPI for comparison between different periods which is required to assess the impact of climate change. To overcome this shortcoming, Dubrovsky *et al*. (2008) introduced the concept of relative drought indices. In order to calculate the relative SPI, the parameters of the Gamma distribution are first estimated for a calibration period. For the purpose of statistical robustness, we use all available years of the RCM simulations up to the year 2000 for calibration (Table I). Future drought conditions are then expressed in terms of the present-day climate by computing the SPI for future precipitation amounts with respect to the Gamma distribution of the calibration period. Therefore, no distributional assumptions for the future period are made. In order to assess the projected changes between baseline and future period, the respective relative SPIs are compared.

The significance of the SPI calculation procedure is evaluated by assessing the goodness-of-fit of the cumulative Gamma distribution function (CDF). Here, the Lilliefors test is used which is a modified version of the Kolmogorov–Smirnov test to account for the situation where the distribution parameters are derived by the same data as used in the test (Crutcher, 1975; Wilks, 1995). The test statistic is defined as the largest absolute difference between empirical and fitted CDFs and the critical values are obtained from Crutcher (1975). Since the critical values are only listed for a few estimated shape parameters of the Gamma distribution, linear interpolation between the specified values is applied. Under the null hypothesis that the theoretical CDF describes the observed data, a significance level (α) of 10% is chosen. The Lilliefors test is calculated for different PRi ($i = 3$, 6, 9, 12, 18, 24 months) of the calibration period and for each month of a year, grid point and RCM separately. Table III lists the percentage of months passing the test at the 10% significance level with respect to all models, months of a year, and grid points within a subregion. The results suggest that the Gamma distribution is a proper theoretical model for *PR3* to *PR18* with more than 90% passing the test. For *PR24*, the values drop below 90%, and even below 80% in the case of BI. This finding is consistent with Guttman (1999) who already stated that the calculation of the SPI with time scales longer than 24 months is problematic due to smaller independent sample sizes. In consideration of this finding and to account for different drought time scales, the SPI3, SPI12, and SPI18 are further analysed. Lloyd-Hughes and Saunders (2002) provide an analysis of correlations between different SPIs of various time scales over Europe. The study reveals that the SPI3 explains 29.2% of the variance in SPI12 and only 16.8% of the variance in SPI18, while the SPI12 explains 72.2% of the variance in SPI18.

Table III. Goodness-of-fit of the two-parameter Gamma distribution. The values indicate the percentage of months passing the Lilliefors test at the 10% significance level with respect to all RCMs, months of a year, and grid points within a subregion.

Subregion	SPI3	SPI6	SPI9	SPI12	SPI18	SPI24
IP	95.4	95.2	94.8	93.5	93.4	92.0
MD	94.9	94.9	94.8	95.0	94.2	92.9
FR	94.2	94.9	95.1	95.1	93.4	87.1
ME	94.2	95.0	95.0	95.4	93.5	84.4
AL	94.1	94.4	94.8	95.1	93.8	86.1
EA	94.5	94.2	93.9	93.7	93.9	91.6
BI	95.1	94.3	94.3	94.8	90.4	73.0
IL	94.0	92.6	94.3	95.1	95.4	93.9
SC	94.5	94.9	95.0	95.3	94.9	90.6
ALL	94.6	94.6	94.6	94.6	93.8	89.3

3.2. Calculation of the self-calibrated Palmer Drought Severity Index

The PDSI opposes atmospheric water supply to soil water demand using a rather simple soil-water balance model (SWBM). The calculation procedure of the PDSI is well documented (e.g. Palmer, 1965; Alley, 1984; Weber and Nkemdirim, 1998) and is only briefly discussed here. However, some specific details with relevance to our study are described in more detail.

Basically, the PDSI calculation procedure can be split into two parts. First, the monthly soil water balance is calculated with the assumption that the upper soil layer can hold 25.4 mm (one inch) and the underlying WHC minus 25.4 mm of water. Monthly potential evapotranspiration (PET) is estimated by monthly mean air temperature following Thornthwaite (1948) and two cases are considered: (1) If precipitation exceeds PET, the surplus is first added to the top layer and then to the bottom layer, and if both layers are saturated, runoff occurs. (2) If precipitation is less than PET, water is extracted from the soil until PET is satisfied or the soil is empty, again starting with the top layer from which water is more easily removed. Since the original version of the SWBM does not account for snow accumulation and snow melt, the calculation of the PDSI during winter and spring in cold regions is problematic (Alley, 1984). To account for this deficiency, a simple snow accumulation and snow-melt model is coupled to the SWBM following van der Schrier *et al*. (2007). In contrast to van der Schrier *et al*. (2007), the standard deviation of daily air temperature is derived for each month and grid point separately. In order to

Copyright © 2011 Royal Meteorological Society

avoid problems associated with the spin-up of the soil water balance, the first 24 months of the SWBM computations are neglected. Palmer (1965) used the long-term output of the SWBM to calculate the 'climatically appropriate for existing conditions (CAFEC)'-precipitation by summing up the potential values of a certain month scaled by the ratio of long-term monthly mean actual to potential values. The Palmer moisture anomaly index (Palmer Z-Index; ZI) is then the difference between monthly precipitation and CAFEC-precipitation, weighted by an empirical derived normalisation factor (the climate characteristic) which accounts for local climate features. Therefore, the ZI measures the deviation from climatically normal soil moisture conditions for the current month without regarding conditions of preceding months.

In the second part of the PDSI calculation, the classified PDSI values are derived (Table IV). Palmer (1965) used the following formula to compute the preliminary PDSI:

$$X_i = 0.897 \cdot X_{i-1} + \frac{1}{3} \cdot ZI_i, \qquad (2)$$

where i denotes the actual month. Palmer (1965) derived the two empirical factors of the equation (the duration factors) by drawing a straight line to the lowest ZI values accumulated over different lengths of time, aiming at representing most extreme dry periods of various lengths. To determine the beginning and ending of dry and wet spells, the weighting procedure proposed by Heddinghaus and Sabol (1991) is applied.

Table IV. Classification of the PDSI and scPDSI.

(sc)PDSI	Class
≥4.00	Extremely wet
3.00 to 3.99	Very wet
2.00 to 2.99	Moderately wet
1.00 to 1.99	Slightly wet
0.50 to 0.99	Incipient wet spell
0.49 to −0.49	Near normal
−0.50 to −0.99	Incipient drought
−1.00 to −1.99	Mild drought
−2.00 to −2.99	Moderate drought
−3.00 to −3.99	Severe drought
≤−4.00	Extreme drought

The transferability of the original Palmer indices to other climatic regions is restricted since the empirical constants are derived from only a few locations in North America (Alley, 1984). In order to account for these limitations, Wells *et al.* (2004) introduced the self-calibrated (scPDSI). The scPDSI dynamically replaces the empirical constants of Palmer (1965) by values based on local climate conditions and, therefore, enhances the spatial comparability (Wells *et al.*, 2004). The modifications encompass the redefinition of the climate characteristic and the calculation of the duration factors. Consequently, the scZI and the scPDSI can be computed. In contrast to Palmer (1965), the duration factors for dry (wet) spells are calculated for each location separately by fitting straight lines to the lowest (highest) ZI values accumulated over various period lengths. For this purpose, Wells *et al.* (2004) present a general form of Equation (2):

$$X_i = (1 - \frac{m}{m+b}) \cdot X_{i-1} \pm 4 \cdot \frac{ZI_i}{m+b}, \qquad (3)$$

where i denotes the actual month, m the slope and b the intercept of the fitted straight lines. Depending on whether dealing with a dry or wet spell, the corresponding fit parameters are then applied to Equation (3).

Furthermore, for climate change assessment, the concept of relative indices must be applied to the scPDSI for the same reasons as for the SPI by calibrating the index in the past (Dubrovsky *et al.*, 2008). After calibration, the scZI and scPDSI are calculated transiently up to 2050 and climate change is assessed by comparing the indices between future and baseline period.

Wells *et al.* (2004) already noted that the accumulated ZI values over various period lengths are better represented by a non-linear function. The left panel of Figure 4 depicts, as an example, the nonlinear dependency of the lowest accumulated ZI values of the calibration period on different period lengths. Although Figure 4

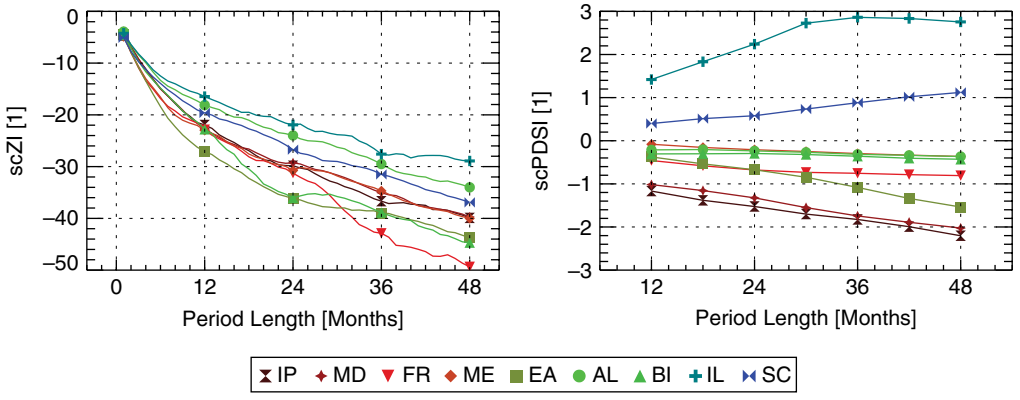

Figure 4. Left panel: Subregional mean of the lowest accumulated ZI values in the calibration period for different period lengths (1–48 months in monthly steps). Right panel: The effect of using different fitting periods (12–48 months in 6 monthly steps) on the mean scPDSI in the future period. Both panels show model no. 6. Ref. text for details. This figure is available in colour online at wileyonlinelibrary.com/journal/joc

Copyright © 2011 Royal Meteorological Society

only illustrates model no. 6 (Table I) and the lowest accumulated ZI values, a similar nonlinear behaviour is also obtained for all other models and for the highest accumulated ZI values (not shown). The nonlinearity can be explained by the fact that ZI values with the opposite sign affect the aggregation for longer period lengths, which consequently results in a transition towards flatter slopes. The right panel of Figure 4 shows the effect of using different period lengths to fit the straight lines on the scPDSI. It can be seen that notable differences between the scPDSI values for short- and long-fitting periods are obtained. Referring to the left panel of Figure 4, this can be related to the nonlinear behaviour of the accumulated ZI values, where shorter period lengths tend to have steeper slopes and smaller intercepts than longer period lengths. According to the autoregressive form of Equation (3), the combined effect is typically that short-fitting periods result in higher weights for the actual ZI value and in lower weights for the previous months. To account for this nonlinearity, Wells *et al*. (2004) proposed to examine the correlation between accumulated ZI values and time before performing the linear regression. Table V summarizes the coefficient of determination (R^2) between accumulated ZI values of the calibration period and time for various period lengths, averaged over all RCMs and grid points within a subregion. Generally, shorter periods show higher R^2 values. Since Palmer (1965) clearly put more weight on representing shorter periods, an initial period length of 24 months is used to derive the fit parameters. Following Wells *et al*. (2004), the last month is repeatedly omitted until a threshold of 0.9 for the correlation coefficient is obtained. In case that the threshold is not achieved until a lower bound of seven months, the scPDSI is not calculated in order to avoid instability.

Vicente-Serrano *et al*. (2010) comprehensively analysed correlations between the SPI and the scPDSI for 11 observational stations worldwide. They found a strong agreement between the scPDSI and the SPI, with maximum values between 0.60 and 0.85 at time scales between 5 and 24 months which is in agreement with previous studies. Furthermore, they analysed correlations between the scPDSI and SPI under a 2 K and 4 K temperature increase and found markedly decreasing correlations since the SPI does not account for the role of air temperature.

Table V. Coefficient of determination (R^2) between accumulated ZI values and time for various period lengths, averaged over all RCMs and grid points within a subregion.

Subregion	Lowest accumulated ZI values			Highest accumulated ZI values		
	Period length (months)			Period length (months)		
	12	24	48	12	24	48
IP	94.1	91.0	84.8	89.3	87.2	78.4
MD	95.2	89.1	86.7	89.9	87.4	83.2
FR	93.0	88.6	79.5	90.6	89.7	80.9
ME	92.6	88.2	78.9	89.3	89.9	85.1
AL	93.0	87.7	80.6	85.7	86.0	79.3
EA	95.4	91.0	82.6	91.0	90.1	86.0
BI	92.5	89.5	80.3	87.8	90.2	85.8
IL	91.4	88.8	82.4	83.0	83.4	78.8
SC	88.7	87.2	83.3	86.3	85.7	82.5
ALL	92.9	89.0	82.7	88.8	88.0	82.8

3.3. Dry and wet event characteristics

Dry and wet events are defined according to the classification of the two drought indices (Tables II and IV), where index values of $+1.00$ (-1.00) mark the transition from normal to wet (dry) conditions. Following McKee *et al*. (1993), the temporal sequence of the drought indices is used to specify dry events as periods where the drought index values are continuously negative and the minimum of the index values during these periods falls below -1.00. Wet events are defined analogous, but with positive drought index values and a threshold of $+1.00$. Changes between baseline and future period in dry and wet event frequency (number of event occurrences), length (number of months during events), distance (number of months between two events), magnitude (sum over the drought indices during events), and area (percentage of grid points affected by events) are further analysed.

3.4. Statistical significance and uncertainty

The statistical significance of the multi-model mean change between baseline and future period is calculated by applying the t-test to the subregional mean values of the 8 models which are seasonally averaged over the two 30-year periods. Since all RCMs are forced towards the observed mean values of the baseline period through model error correction, the independent one-sample t-test is used for air temperature and precipitation. Here, the null hypothesis is tested if the distribution across all models in the future period has the same mean as the average over the error corrected models in the baseline period. In contrast, the drought indices show pronounced variation of the mean values since calibration and baseline period are not identical. Therefore, the two-sided t-test for paired samples is used to assess the significance of the multi-model mean change, under the null hypothesis that the distributions of future and baseline values across all models have the same mean. The application of the t-test assumes independent and identically distributed samples which are normally distributed. The assumption of normality in our study is justified by the central limit theorem since multiple averaged quantities are applied. Furthermore, we detected no substantial deviations from normal distribution applying the Shapiro–Wilk test.

In order to test the statistical significance of the changes in interannual variability between baseline and future period, components of variation due to spatial variability are excluded by using subregional averaged time series of each model. An unbiased comparison of interannual variability is achieved by removing a

Copyright © 2011 Royal Meteorological Society

linear trend from the seasonal mean values of both periods (Räisänen, 2002). As a measure for interannual variability, the mean of the squared deviations of the seasonal values from the linear fit (mean-squared error; MSE) is further used and the projected changes are calculated as ratios between future and baseline MSE. The pooled residuals of the eight models are used to assess the statistical significance of the seasonal changes in interannual variability. The pooled residuals partly show severe deviations from normality and, therefore, the Fligner–Killeen test is applied which proofed to be most robust against non-normally distributed data (Conover *et al*., 1981).

Significance levels lower than 1, 1–5, 5–10 and greater than 10% are termed as highly significant, significant, weakly significant and insignificant, respectively.

Uncertainties of the projected changes are quantified by two different measures. First, the inter-model standard deviation is calculated. With the information of the multi-model mean change, probabilities of the projected changes can be derived. According to the normal distribution, about 68% of the climate change signals lie within ± 1 standard deviation, while already about 95% lie within ± 2 standard deviations. Second, the percentage of models which coincide in the sign of change is calculated as a nonparametric uncertainty measure. Applying the confidence terminology of the 4th Assessment Report of the Intergovernmental Panel on Climate Change (IPCC 4AR; Solomon *et al*., 2007), very high confidence, high confidence, and medium confidence are reached if at least 90% (in our study all 8 models), at least 80% (6 models), and at least 50% (4 models) coincide in the sign of change, respectively.

4. Results and discussion

4.1. Changes in the mean, their significance, and uncertainty

For air temperature, Figure 5 displays maps of the error corrected seasonal multi-model mean change between baseline (1961–1990) and future (2021–2050) period over Europe. Air temperature changes are positive in all seasons, and the most responsive regions are the north-eastern parts of Europe in winter and southern Europe in summer. The centred values in each box of Figure 9 indicate the seasonal multi-model mean changes of the nine subregions. The magnitude of the change is lowest for IL in summer with +1.04 K while the most sensitive regions (SC in winter and MD in summer) show a warming of +2.43 K. The brightness of the colours of Figure 9 represents the level of significance of the *t*-test. It can be seen that highly significant shifts towards increasing air temperature are obtained for all seasons and subregions. Concerning the uncertainty of the changes, all models agree in increasing air temperature (lower left values in each box of Figure 9) and, therefore, very high confidence can be attributed to the changes for all seasons and subregions. The inter-model standard deviation (lower right values in each box of Figure 9) is a factor two to three (even more for some cases) smaller than the multi-model mean change, underpinning high confidence of the projected changes.

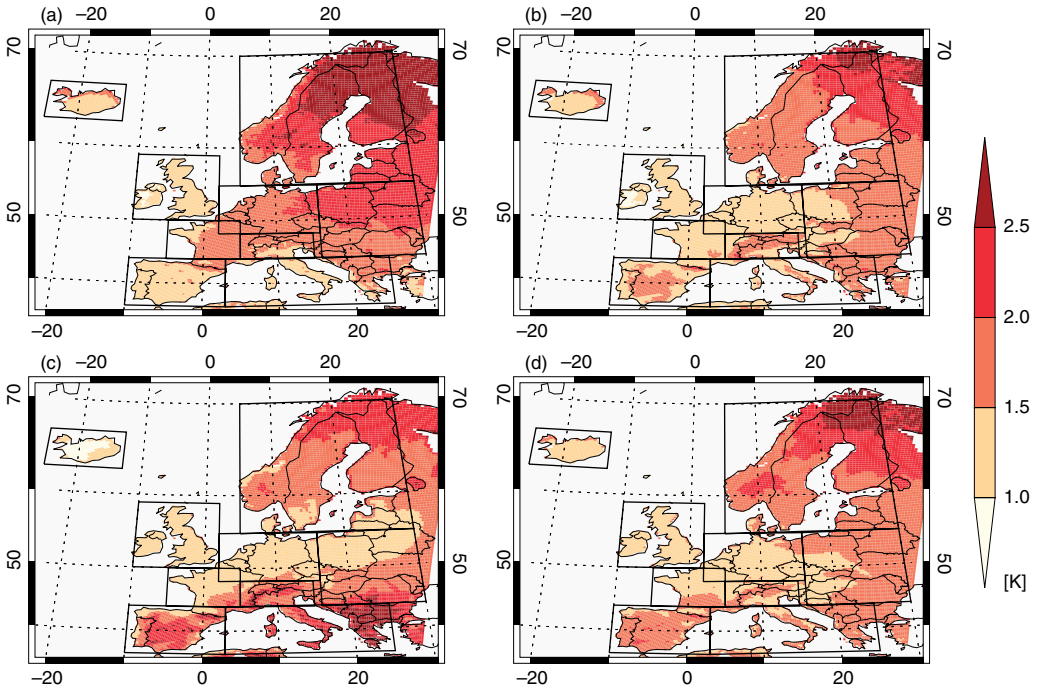

Figure 5. Multi-model mean change between 1961 and 1990, and 2021 and 2050 of the error-corrected RCMs for seasonal mean air temperature for: (a) winter (DJF), (b) spring (MAM), (c) summer (JJA), and (d) autumn (SON). This figure is available in colour online at wileyonlinelibrary.com/journal/joc

Copyright © 2011 Royal Meteorological Society

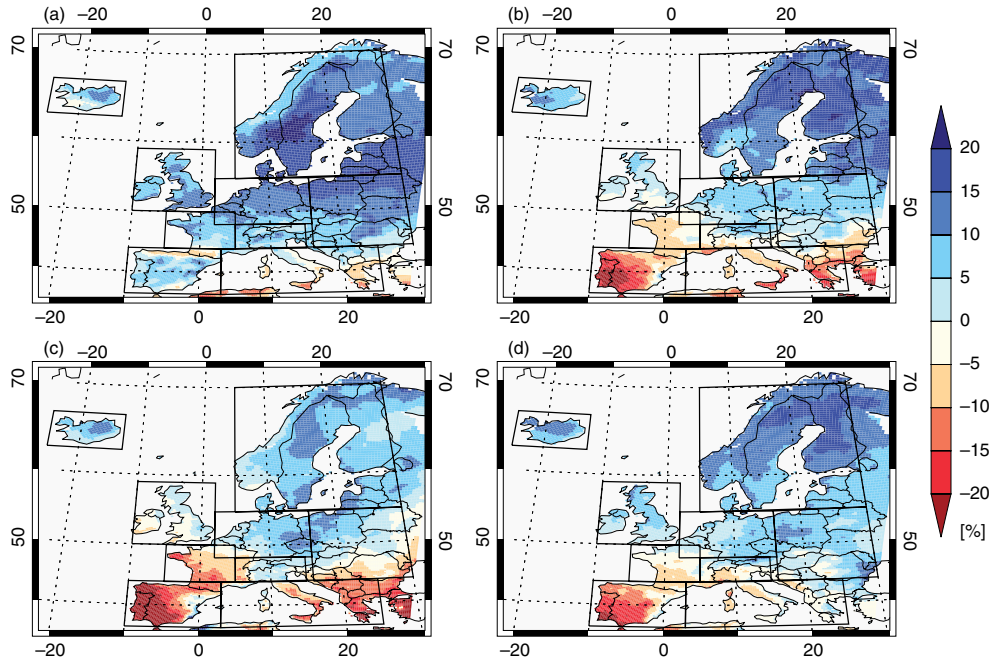

Figure 6. Same as Figure 5 but for precipitation. This figure is available in colour online at wileyonlinelibrary.com/journal/joc

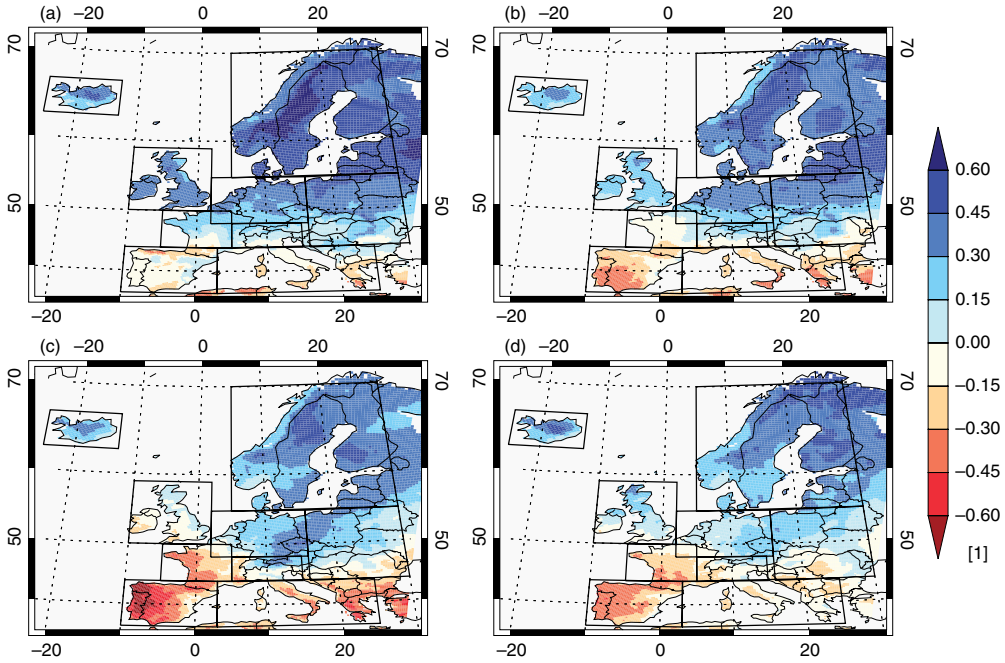

Figure 7. Same as Figure 5 but for the SPI3. This figure is available in colour online at wileyonlinelibrary.com/journal/joc

For precipitation and the SPI3, maps of the seasonal changes over Europe are shown in Figures 6 and 7, respectively. Both changes clearly indicate a gradient from drier conditions in southern to wetter conditions in northern Europe, showing a northward shift of areas with reduced precipitation from winter to summer. Figure 9 lists the seasonal changes of precipitation and all calculated SPIs on subregional basis. The largest changes towards drier and wetter conditions are obtained for the southernmost (IP and MD) and northernmost (IL and SC) subregions, respectively. For precipitation, the most pronounced changes are found for IP in summer and for SC in winter with −17.2% and +14.6%, respectively. For the SPIs, the changes are expressed in terms of standard deviations and are mostly smaller (larger) than −0.5 (+0.5) for IP and MD (IL and SC). Most subregions show larger changes for SP12 and SPI18 than for SPI3, which are accompanied by lower interseasonal variation. Both precipitation and the SPIs indicate highly significant changes for the southern- and northernmost subregions in most seasons. For FR, significant changes towards drier

Copyright © 2011 Royal Meteorological Society

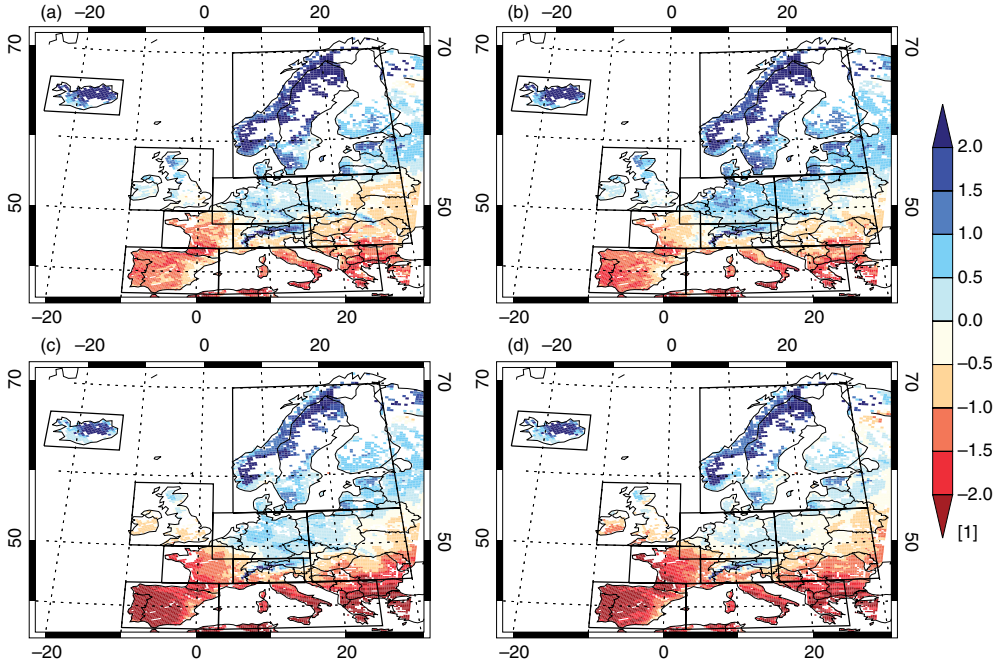

Figure 8. Same as Figure 5 but for the scPDSI. White areas represent missing values due to missing soil data or infeasibility of the scPDSI calculation procedure (Ref. text for details). This figure is available in colour online at wileyonlinelibrary.com/journal/joc

conditions are found in spring and summer for precipitation and SPI3. ME, EA, and BI show significant to highly significant changes towards wetter conditions for all SPIs in winter and spring. In summer and autumn, significant changes are mainly obtained for the long-term SPIs (SPI12 and SPI18). Concerning the uncertainty of the changes, quite a similar spatial pattern is found with high to very high confidence in the sign of change for the southern- and northernmost subregions. For FR and AL, only medium confidence is obtained in most seasons, while ME, EA, and BI mainly show high confidence of the changes.

For the scPDSI, maps of the seasonal changes over Europe are illustrated in Figure 8. The missing values in the northern part of Europe are predominantly due to missing values of required soil moisture storage capacity. The scPDSI shows again a strong gradient of the projected changes from pronounced drier conditions in southern to wetter conditions in northern European regions in all seasons. Generally low interseasonal variation is observed. Figure 9 summarizes the seasonal changes for the scZI and the scPDSI on subregional basis. The most pronounced changes for both indices are again observed for the southern- and northernmost subregions with a shift towards drier and wetter conditions in most seasons, respectively. The maximum changes of the scPDSI are observed in summer (spring) for IP and MD (IL and SC), indicating a shift in the order of two scPDSI units. The scZI shows the most pronounced shifts towards wetter conditions in autumn (winter) for IL (SC). In contrast to the other indices, negative scZI values are obtained for all subregions in summer. Highly significant changes for both indices are obtained for southern (IP, MD, and FR) and northern (IL and SC) Europe in most seasons. For regions in between, the level of significance is seasonal varying and mostly indicates lower significant changes than in southern and northern Europe. Concerning the uncertainty of the changes, high to very high confidence in the sign of change can be attributed to the changes of IP, MD, FR, IL, and SC in most seasons. The remaining subregions mostly show lower confidence in the sign of change, which is in good accordance with the findings for the significance level.

The spatial differences of air temperature in winter can be largely explained by the modest warming of the ocean influencing the maritime climate of western Europe in combination with altered snow–albedo feedback mechanisms in northern and eastern Europe (Rowell, 2005). The high summer temperatures in the south can be related to an earlier and more rapid reduction of soil moisture in spring (e.g. Wetherald and Manabe, 1995; Gregory *et al*., 1997). The obtained spatial pattern of the precipitation changes is common to climate simulations and identified as the European Climate change Oscillation (ECO) which can be related to a seasonal dependent northward shift of the mid-latitude storm track (Giorgi and Coppola, 2007). Differences between the changes of precipitation and the different SPIs highlight the importance of investigating different time scales of precipitation amounts. The low interseasonal variation of the mean scPDSI can be explained by the autoregressive form of the index and hence by the memory on soil moisture conditions of preceding months. Areas which are affected by a drying tendency according to the scPDSI have a larger northward extent compared to precipitation and the SPI3. This can be related to a drier soil as a result of increasing air temperature. Even though for some regions wetter

Copyright © 2011 Royal Meteorological Society

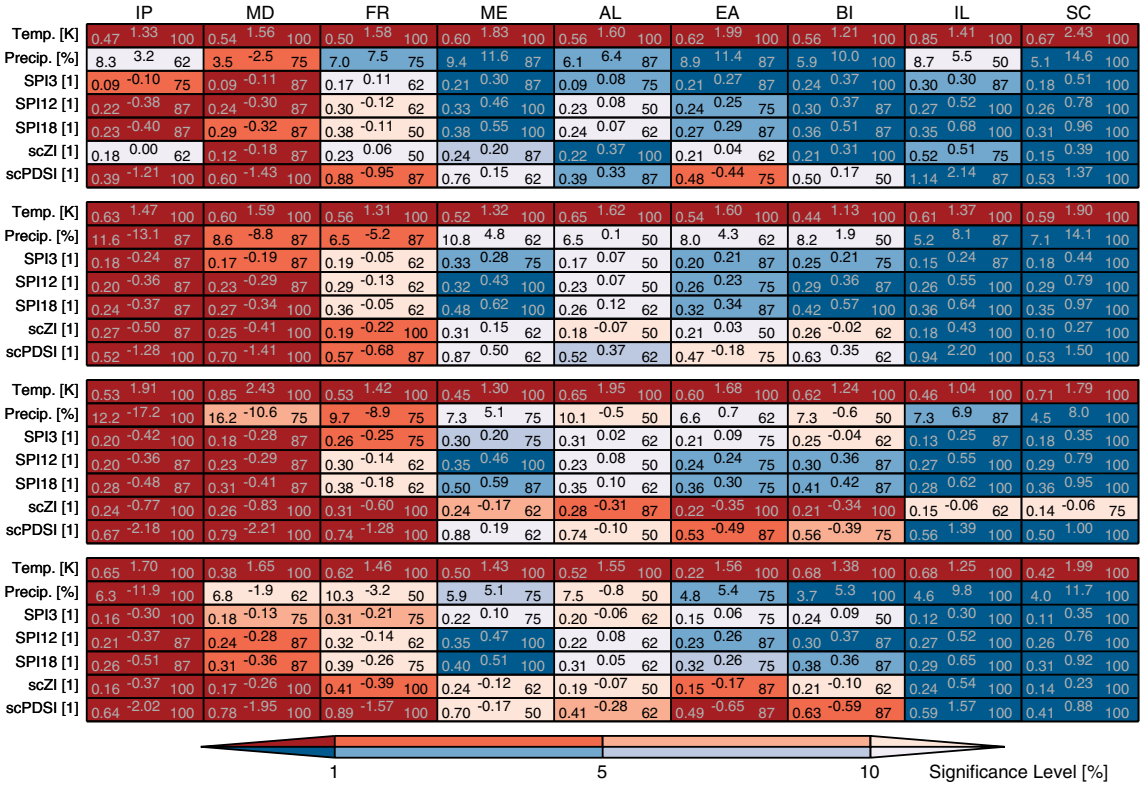

Figure 9. Seasonal changes in the mean between 1961 and 1990, and 2021 and 2050. The brightness of the colours represents the level of significance of the *t*-test. Red (blue) colours illustrate drier (wetter) conditions in the future period. Multi-model mean change is given in the upper centre of each box. Intermodel standard deviation and percentage of models which coincide with the sign of the multi-model mean change are given in the lower left and right of each box, respectively. This figure is available in colour online at wileyonlinelibrary.com/journal/joc

summer and autumn conditions are observed for precipitation and the SPIs, increasing air temperature causes drier soil moisture conditions and, therefore, negative scZI values (e.g. ME, EA, and BI). In winter, large positive scZI values are obtained in regions with low precipitation increases (e.g. AL and IL), indicating that additional moisture is added to the soil with respect to the baseline period which can be related to the effect of lower snow accumulation and higher snow melt due to increasing air temperature. Since both drought indices are approximately centred at zero in the baseline period, changes in the mean can be linked to shifts in the classification of the two indices (Tables II and IV). Especially the scPDSI indicates pronounced changes with a shift towards 'mild/moderate drought' ('slightly/moderately wet') conditions for southern (northern) European regions with respect to the present-day climate.

4.2. Changes in interannual variability, their significance, and uncertainty

Figure 10 summarizes the seasonal changes in interannual variability, their statistical significance and uncertainty for the nine subregions.

For air temperature, increasing interannual variability is obtained for the southern and southeastern European subregions IP, MD, and EA in all seasons. The strongest increase is obtained for IP in autumn with +50.5%. Seasonally, also decreasing variability is projected, most pronounced in winter, and for BI and IL with −24.3% to −35.1%. The brightness of the colours of Figure 10 represents the level of significance of the Fligner–Killeen test. Significant changes are observed for only a small proportion and are in good accordance with the most pronounced changes in magnitude. Concerning the uncertainty of the changes, high confidence in the sign of change (lower right values in each box of Figure 10) is mainly obtained in winter and spring for regions where interannual variability decreases (FR, BI, and IL).

For precipitation and the SPIs, mainly increasing interannual variability is obtained, except for IL and partially for BI. The largest increases are found for SPI3 in spring with +76.9% and +72.3% for IP and FR, respectively. Interestingly, subregions with the most pronounced decreases in the mean for precipitation and the SPIs (IP and MD) show increasing interannual variability. IL shows the most pronounced decreases for SPI12 and SPI18 with a magnitude in the order of −20% to −30%. In some regions and seasons, opposite signs of the changes for the different SPIs are obtained (e.g. BI in spring). Significant changes are mainly obtained for IP and SC with increasing, and for IL with decreasing interannual variability. However, different SPIs often feature different levels of significance, e.g. for IP, BI, and IL mostly higher significance levels for the SPI12 and SPI18 are obtained. Concerning the uncertainty, the inter-model standard deviation is in most cases clearly larger than the multi-model mean change. This is in line with the number of models which show the same sign

Copyright © 2011 Royal Meteorological Society

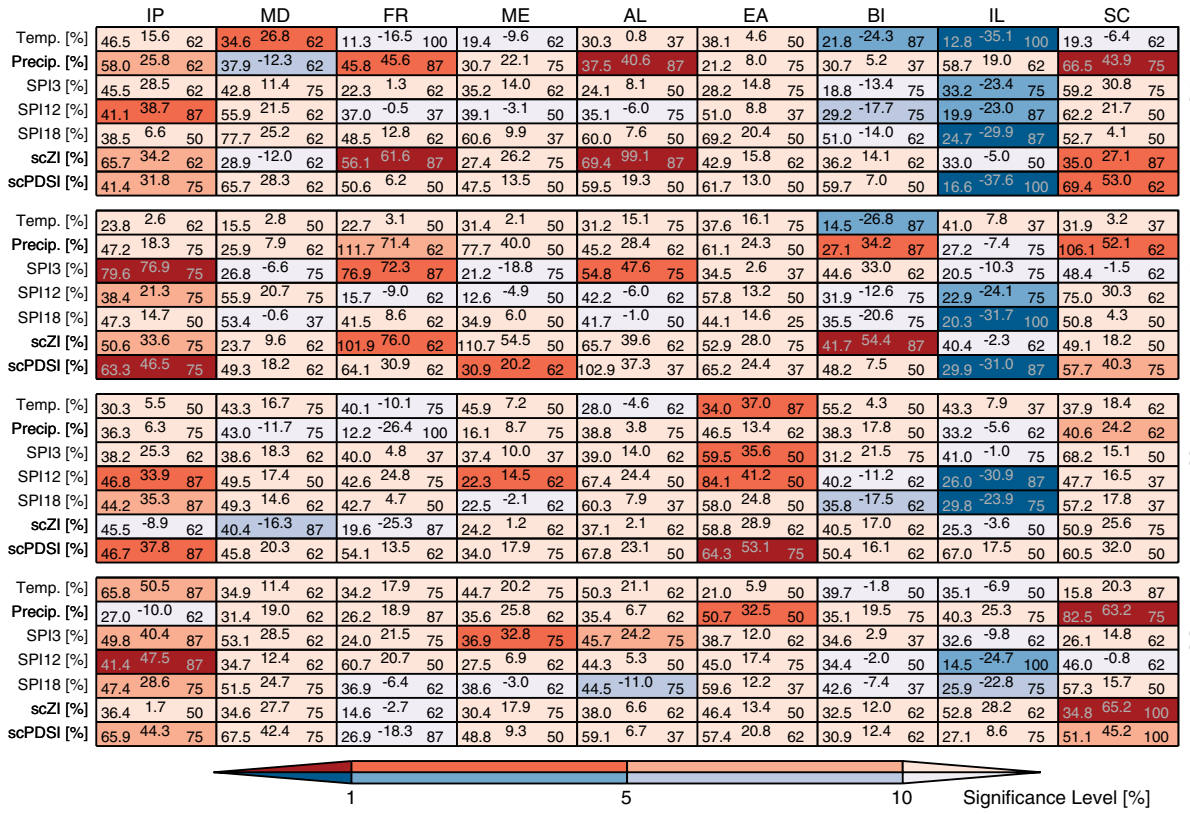

Figure 10. Seasonal changes in interannual variability between 1961 and 1990, and 2021 and 2050. The brightness of the colours represents the level of significance of the Fligner–Killeen test. Red (blue) colours illustrate higher (lower) interannual variability in the future period. Multi-model mean change is given in the upper centre of each box. Intermodel standard deviation and percentage of models which coincide with the sign of the multi-model mean change are given in the lower left and right of each box, respectively. This figure is available in colour online at wileyonlinelibrary.com/journal/joc

of change, indicating that only about 40% indicate high confidence of the changes.

For the scZI and scPDSI, increasing interannual variability is obtained for most subregions and seasons. The largest increases for the scZI (scPDSI) are found for AL in winter (EA in summer) with +99.1% (+53.1%). IL again represents an exception with pronounced decreases in winter and spring for the scPDSI with −37.6% and −31.0%, respectively. Weakly to highly significant changes of both indices towards higher interannual variability are observed for IP (SC) in winter and spring (winter and autumn). IL shows high significance for the decreasing variability of the scPDSI. Generally, large uncertainties in the magnitude and in the sign of the changes are obtained.

The findings are consistent with previous studies (e.g. Räisänen, 2002; Rowell, 2005; Giorgi and Coppola, 2009) where the decreasing temperature variability in winter in cold regions is attributed to dampened snow–albedo feedback mechanisms due to reduced snow cover. Increases in summer temperature variability can be partly attributed to amplified soil moisture–temperature feedbacks for drier soil conditions (Giorgi and Coppola, 2009). The increasing interannual variability of precipitation can be related to a more intense hydrological cycle and amplified soil moisture–precipitation feedbacks (Giorgi and Coppola, 2009). Generally, the observed patterns are more pronounced by the end of the 21st century (Giorgi and Coppola, 2007). Significantly increasing interannual variability is projected in regions with pronounced changes in the mean towards wetter (SC) as well as towards drier (IP) conditions. Changes in interannual variability vary substantially among models, indicating generally less confident climate change signals than those obtained for the changes in the mean. The importance of investigating different time scales of precipitation amounts is highlighted in various regions. For some cases, significant changes are obtained although the models reveal low concordance in the sign of change, indicating substantial differences between the individual models in the projected changes of interannual variability since the Fligner–Killeen test is applied to the pooled residuals of the eight models.

4.3. Changes in dry and wet event characteristics, their significance, and uncertainty

Figures 11 and 12 summarize the projected changes in mean dry and wet event frequency, length, distance, magnitude, and area, their statistical significance and uncertainty in the nine subregions. In order to provide more detailed information on projected distributional changes, Figures 13 and 14 depict quantile–quantile-plots (QQ-plots) for the distributions of dry and wet event characteristics in the baseline and future period.

Copyright © 2011 Royal Meteorological Society

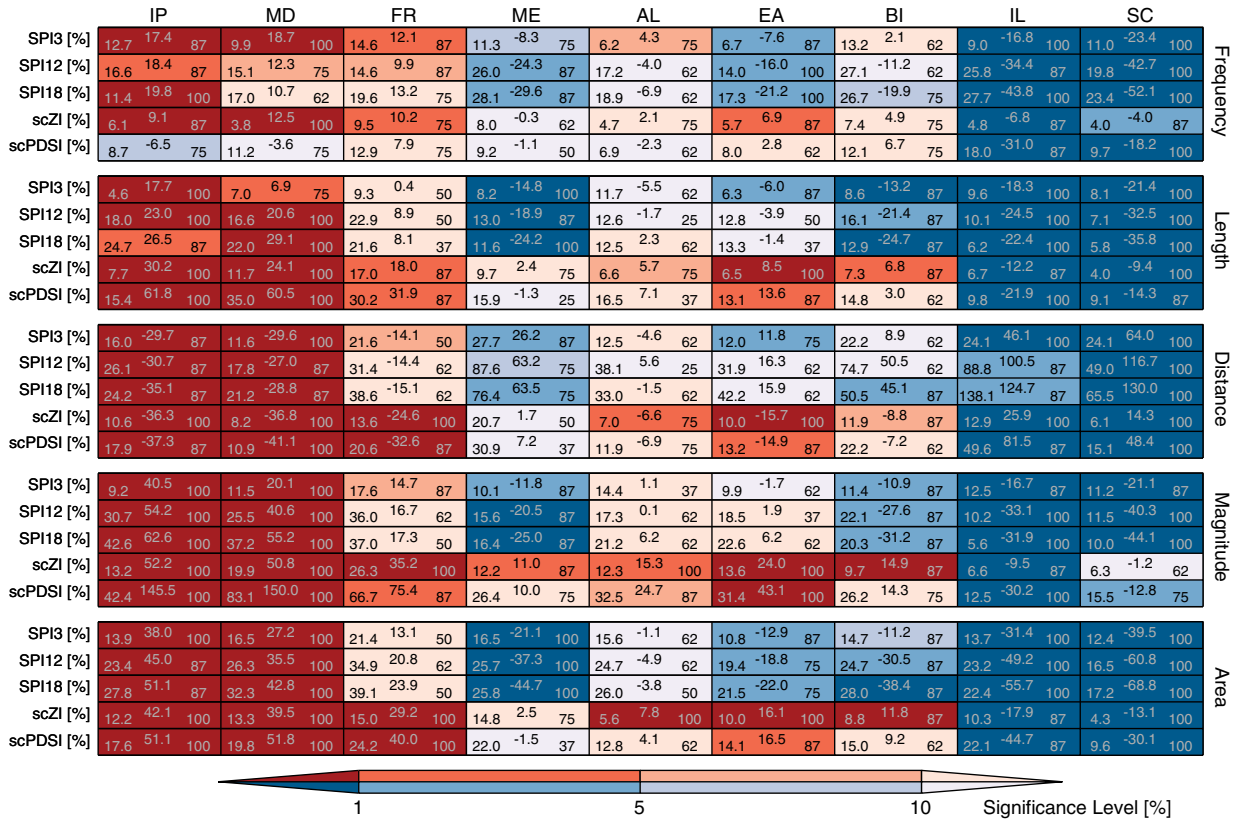

Figure 11. Changes in mean dry event frequency, length, distance, magnitude, and area between 1961 and 1990, and 2021 and 2050. The brightness of the colours represents the level of significance of the *t*-test. Red (blue) colours illustrate drier (wetter) conditions in the future period. Multi-model mean change is given in the upper centre of each box. Intermodel standard deviation and percentage of models which coincide with the sign of the multi-model mean change are given in the lower left and right of each box, respectively. This figure is available in colour online at wileyonlinelibrary.com/journal/joc

For the SPIs, Figure 11 reveals that the most pronounced increases in mean dry event frequency, length, distance, magnitude, and area are obtained for the southernmost subregions MD and, even more pronounced, IP. In most cases, the SPI indicates a gradient towards a higher magnitude of change for the long-term SPIs. For example, the SPI18 indicates in IP increasing mean dry event frequency by +19.8%, length by +26.5%, magnitude by +62.6%, and area by +51.1%, while distance decreases by −35.1%. FR and ME mark the transition zone from drier to wetter conditions. Figure 12 depicts that the northernmost subregions IL and SC show the most pronounced changes towards wetter conditions. The largest changes are again observed for the long-term SPIs. For example, the SPI18 indicates in SC an increase of mean wet event frequency by +23.1%, length by +77.5%, magnitude by +170.1%, and area by +113.2%, while distance decreases by −62.0%. From Figures 11 and 12 it can be seen that mostly highly significant changes are found for the southern- and northernmost subregions. Significant changes towards higher frequency, lower distance, and larger magnitude of dry events are obtained for the SPI3 in FR. ME shows weakly to highly significant decreases (increases) of all investigated dry (wet) event characteristics. For AL, mainly insignificant changes are obtained regarding all analysed dry and wet spell characteristics. Concerning the uncertainty of the changes, the southern- and northernmost subregions show high accordance between models in the sign of change, indicating high to very high confidence. The inter-model standard deviation indicates a fairly large spread among models which is most pronounced for the long-term SPIs. However, the inter-model standard deviation is clearly lower than the multi-model mean change, underpinning high confidence of the projected changes. Figures 13 and 14 reveal that the changes of the SPIs are strongly pronounced for the upper percentiles of the distributions, mainly for event length, distance, magnitude, and especially for the long-term SPIs. Severe changes in the extremes arise particularly for the southern- and northernmost subregions. For example, the SPI18 indicates for IP changes in the 95th percentile for dry event frequency of +0.9 (+11.7%), length of +10.6 months (+19.5%), distance of −36.0 months (−37.0%), and magnitude of +38.5 (+66.8%). Therefore, the relative changes in the 95th percentile for dry event distance and magnitude are even more pronounced than the changes in the mean. In SC, the SPI18 indicates changes in the 95th percentile for wet event frequency of +1.1 (+15.5%), length of +62.5 months (+127.5%), distance of −77.8 months (−61.0%), and magnitude of

Copyright © 2011 Royal Meteorological Society

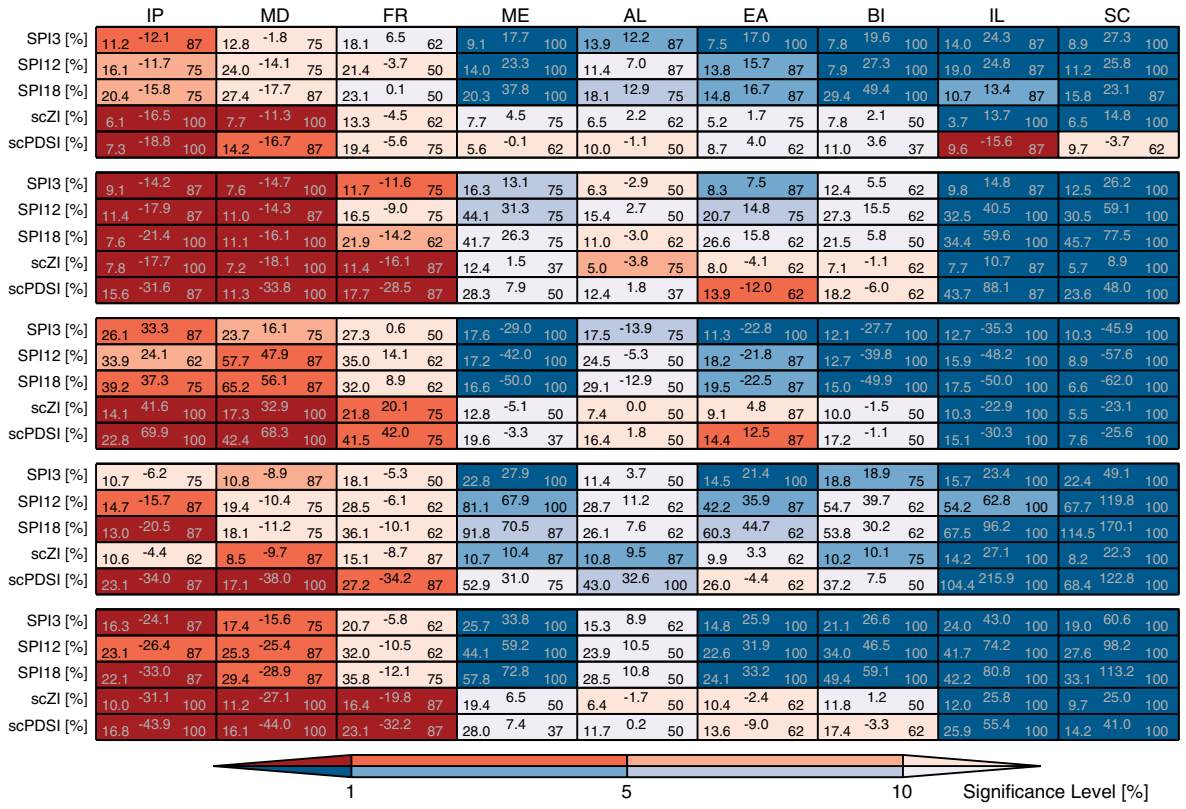

Figure 12. Same as Figure 11 but for wet events. This figure is available in colour online at wileyonlinelibrary.com/journal/joc

+138.1 (262.7%). Again, the relative changes in the 95th percentile for wet event length and magnitude are even more pronounced than the changes in the mean. The distributional changes of event area for the southern- and northernmost subregions show a pronounced shift of the distribution towards larger areal fraction affected by dry and wet events. Distinct changes are observed at the centre of the distributions. This can be related to a decrease in the frequency of lower areal fractions (indicated by steep slopes at lower quantiles), which is accompanied by an increase in the frequency of larger areal fractions (indicated by flat slopes at higher quantiles).

For the scZI and scPDSI, Figure 11 depicts that the largest increases of mean dry event length, distance, magnitude, and area are again found for the southernmost subregions IP and MD. Here, the scPDSI shows a higher magnitude of change than the scZI except for dry event frequency. For example, the scPDSI indicates in IP increasing mean dry event length by +61.8%, magnitude by +145.5%, area by +51.1%, and decreasing frequency and distance by −6.5% and −37.3%, respectively. Figure 12 reveals that the northernmost subregions IL and SC show the most pronounced changes towards wetter conditions. In SC, the scPDSI indicates increasing mean wet event length by +48.0%, magnitude by +122.8%, area by +41.0%, and a decrease in frequency and distance by −3.7% and −25.6%, respectively. Concerning the significance of the projected changes, mostly highly significant changes are found for the southern- and northernmost subregions. FR exhibits significant changes towards longer, more severe, clustered, and widespread dry events for both indices. For ME, the changes are insignificant except for increasing dry and wet event magnitude of the scZI. AL, EA, and BI indicate significant increases of dry event length, magnitude, and area mainly for the scZI. Concerning the uncertainty of the changes, high to very high confidence in the sign of change is observed for IP, MD, FR, IL, and SC in most cases. For the other subregions, generally lower confidence in the sign of change is obtained. Exceptions are observed e.g. in EA, where high to very high confidence for increasing dry event length, magnitude, and area is obtained. Figures 13 and 14 reveal that the changes for the scZI and scPDSI are again strongly pronounced for the upper percentiles of the distributions, mainly for event length, distance, and magnitude. Severe changes in the extremes arise particularly in the southern- and northernmost subregions and for the scPDSI. For example, the scPDSI shows for IP changes in the 95th percentile for dry event frequency of +1.1 (−3.5%), length of +14.3 months (+65.1%), distance of −13.4 months (−45.7%), and magnitude of +87.6 (+134.8%). Therefore, the relative changes in the 95th percentile for dry event length and distance are even more pronounced than the changes in the mean. In SC, the scPDSI indicates changes in the 95th percentile for wet event frequency of +0.5 (+1.5%), length of +12.0 months (+60.4%), distance of −7.8 months (−28.2%), and magnitude of +59.6 (114.8%). Again, the relative changes in the 95th percentile for wet event length and distance are even

Copyright © 2011 Royal Meteorological Society

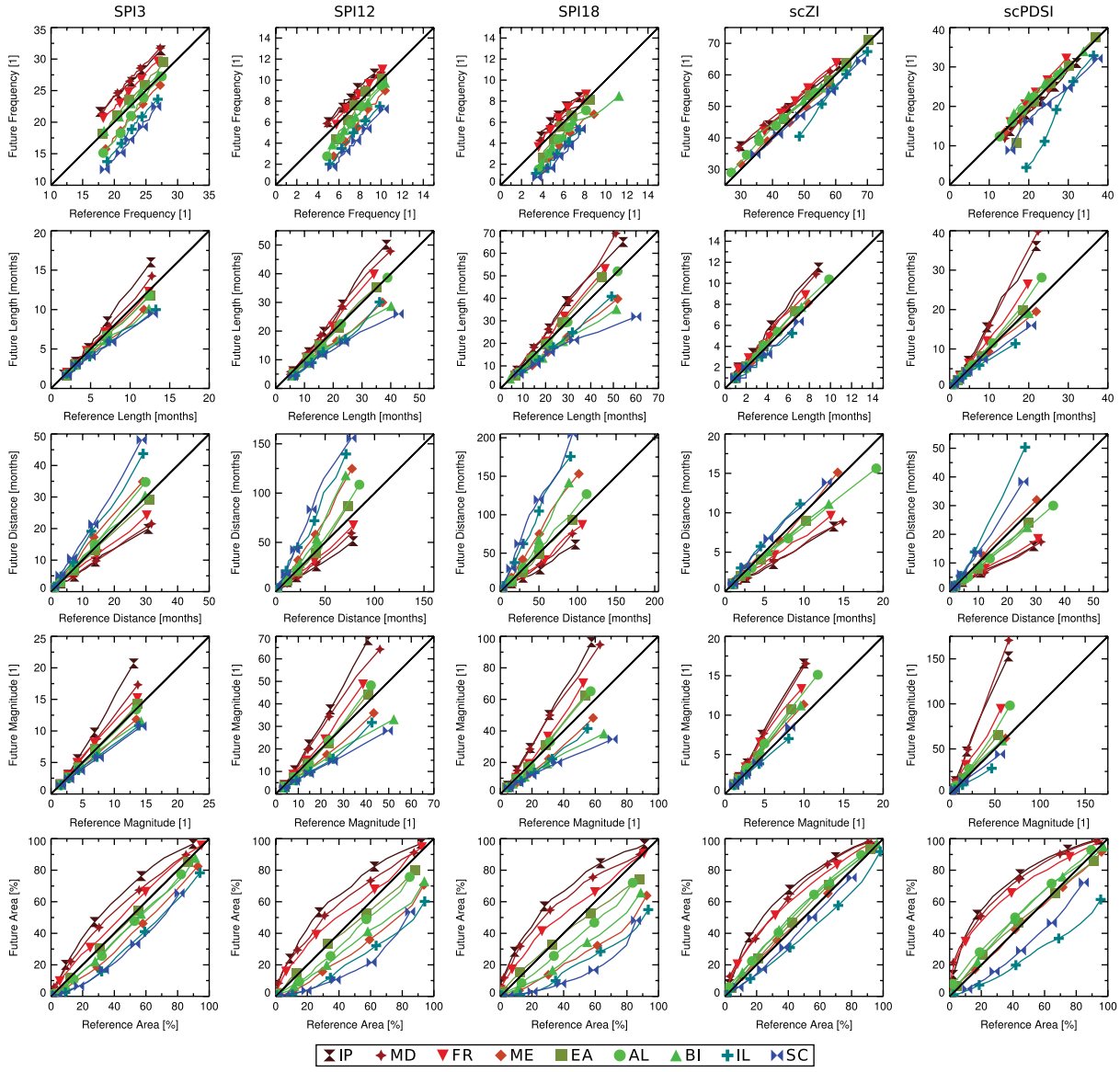

Figure 13. QQ-plots for the baseline (1961–1990) and future (2021–2050) distributions of dry event frequency, length, distance, magnitude, and area for each subregion. The calculation of the quantiles includes all grid points (for frequency) and events (for length, distance, and magnitude) in a subregion. The symbols indicate the 5th, 25th, 50th, 75th, and 95th percentile. Please take note of the different axes scales. This figure is available in colour online at wileyonlinelibrary.com/journal/joc

more pronounced than the changes in the mean. The distributional changes of event area for the southern- and northernmost subregions reveal a pronounced shift of the distribution towards larger areal fraction affected by dry and wet events. The distinct shift of the centre of the distributions can be again related to decreasing frequency of lower areal fractions and increasing frequency of larger areal fractions.

The observed differences in projected dry and wet event characteristics between the SPIs and the Palmer indices can be related to drier soil moisture conditions due to increasing air temperature. The projected changes for the scPDSI are a factor two to three (or even more) larger than for the scZI, especially for the southern- and northernmost subregions. Since the scPDSI takes into account soil moisture conditions of preceding months, this can be explained by consecutive seasonal negative (positive) scZI values which cause extensively low (high) scPDSI values (Figure 9). Furthermore, different signs between the changes of the scZI and scPDSI are obtained for some regions. For example, the scZI indicates shorter wet events for AL which can be explained by the sequence of wetter conditions in winter, followed by drier conditions for the remaining seasons (Figure 9). Owing to the low scZI values in winter, wetter conditions are additionally observed in spring for the scPDSI and, therefore, longer wet events are obtained for some of the models.

5. Summary and conclusions

In this study, a set of eight recent RCM simulations provided by the ENSEMBLES project was used to analyse changes in dry and wet conditions in Europe by

Copyright © 2011 Royal Meteorological Society

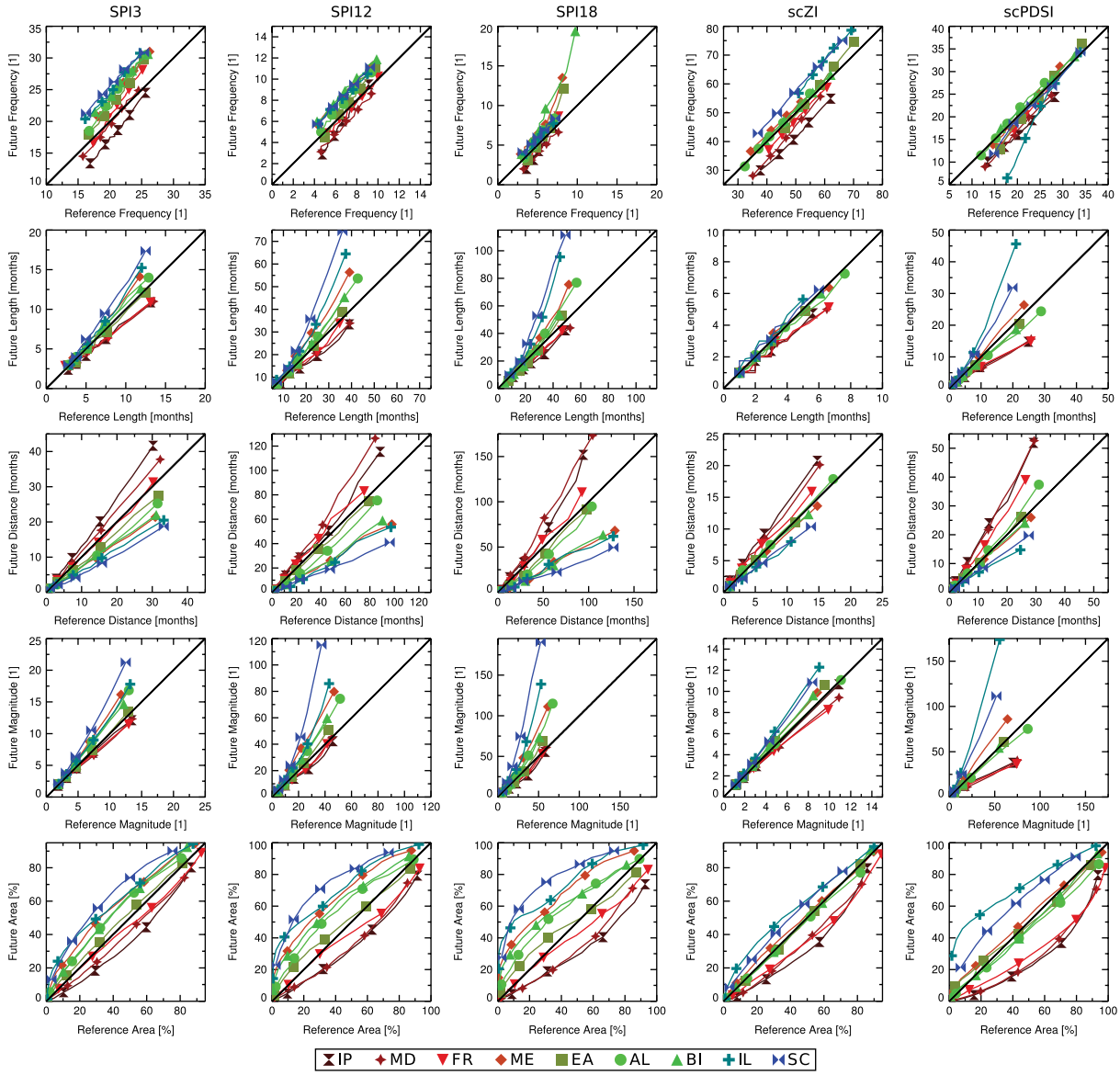

Figure 14. Same as Figure 13 but for wet events. This figure is available in colour online at wileyonlinelibrary.com/journal/joc

the mid of the 21st century under the A1B emission scenario. A quantile-based empirical statistical error-correction approach was applied to modelled daily mean air temperature and precipitation amount to account for RCM errors, and commonly used drought indices – SPI, scZI and scPDSI – were calculated. Changes in the mean, in interannual variability and in frequency, length, distance, magnitude, and area of dry and wet events were investigated. The statistical significance of the projected multi-model mean changes and the according uncertainties were analysed for nine European subregions. Furthermore, distributional changes of the dry and wet spell characteristics were assessed. The key findings can be summarized as follows:

(1) Changes in the mean: Air temperature shows highly significant and confident increases for all of Europe and all seasons. Precipitation and the drought indices indicate the most pronounced changes towards drier and wetter conditions in the southern- and northernmost subregions, respectively. Here, the changes are highly significant and confident in most seasons. In other regions, the changes are more diverse. Opposite directions between the changes of the SPIs and the Palmer indices are obtained due to the effect of increasing air temperature, revealing a drying tendency of the scZI and scPDSI mainly in summer and autumn. Changes of the long-term drought indices are generally more pronounced than those of the short-term indices, highlighting the importance of investigating different time scales of drought.

(2) Changes in interannual variability: The projected changes in interannual variability are less significant and confident than the changes in the mean. Significantly increasing interannual variability is projected in regions with pronounced changes in the mean towards wetter as well as towards drier conditions.

Copyright © 2011 Royal Meteorological Society

Significantly and confidently decreasing interannual variability is mainly expected in Iceland.

(3) Changes in dry and wet event characteristics: As for the changes in the mean, the most pronounced increases in dry (wet) event frequency, length, sequence, magnitude, and area are expected for the southernmost (northernmost) European subregions. Here, the changes are highly significant and highly confident for most drought indices. For the other subregions, substantial differences between the SPIs and the Palmer indices are obtained concerning the sign, the significance, and the confidence of the changes. Here, a tendency towards increasing dry event frequency, length, sequence, magnitude, and area is mainly obtained for the scZI and scPDSI due to the effect of increasing air temperature. The long-term drought indices show a stronger response to climate change than the short-term indices. Severe changes in the extremes of event length, distance, and magnitude particularly arise in the southern- and northernmost subregions regarding all investigated drought indices. Furthermore, the distributional changes of event area reveal a pronounced shift towards larger areal fraction affected by dry and wet events.

It can be concluded that significant changes in dry and wet event characteristics are expected with high confidence in the southernmost (mainly France, Italy, and Spain) and northernmost (mainly Iceland and Scandinavia) regions of Europe. We demonstrated that the role of increasing air temperature as well as the considered time scale of drought plays an important role for the assessment of future drought conditions. The recently introduced Standardised Precipitation-Evapotranspiration Index (Vicente-Serrano, 2010) comprises both aspects and, therefore, represents a valuable supplement to the commonly used SPI and scPDSI for future studies. Although the comparability to other studies is restricted due to different climate model ensembles, emission scenarios, time horizons, or drought indices, our study is in agreement with previous studies and adds confidence to the expectation that southern Europe is most probably facing an increased risk of longer, more frequent, severe, and widespread droughts, while northern Europe is facing increased risk of intensified wet events. These changes are expected to be particularly pronounced with regard to extreme events. A broad spectrum of impacts can be expected from these changes, and it is highly advisable to develop appropriate water management and adaptation strategies. Outside of these high-risk regions, the projected changes are more dissonant and less reliable, but cannot be ruled out. This uncertainty is particularly challenging and calls for flexible and adaptable water management strategies.

Acknowledgements

The ENSEMBLES data used in this work was funded by the EU-FP6 integrated project ENSEMBLES (Contract number 505539; http://ensembles-eu.org) whose support is gratefully acknowledged. We acknowledge the E-OBS dataset from the ENSEMBLES project and the data providers in the ECA&D project (http://eca.knmi.nl). This work was partly funded in the framework of the EU-FP7 project ACQWA (Contract number 212250; http://acqwa.ch) whose support is gratefully acknowledged.

References

Abramowitz M, Stegun I. 1965. *Handbook of mathematical functions, with formulas, graphs, and mathematical tables*. Dover Publications: New York.

Alley WM. 1984. The Palmer drought severity index: limitations and assumptions. *Journal of Climate and Applied Meteorology* **23**: 1100–1109.

Beniston M, Stephenson DB, Christensen OB, Ferro CAT, Frei C, Goyette S, Halsnaes K, Holt T, Jylhä K, Koffi B, Palutikof J, Schöll R, Semmler T, Woth K. 2007. Future extreme events in European climate: an exploration of regional climate model projections. *Climatic Change* **81**: 71–95, DOI: 10.1007/s10584-006-9226-z.

Blenkinsop S, Fowler HJ. 2007. Changes in European drought characteristics projected by the PRUDENCE regional climate models. *International Journal of Climatology* **27**: 1595–1610, DOI: 10.1002/joc.1538.

Bonaccorso B, Bordi I, Cancelliere A, Rossi G, Sutera A. 2003. Spatial Variability of drought: an analysis of the SPI in Sicily. *Water Resources Management* **17**: 273–296.

Briffa KR, van der Schrier G, Jones PD. 2009. Wet and dry summers in Europe since 1750: evidence of increasing drought. *International Journal of Climatology* **29**: 1894–1905, DOI: 10.1002/joc.1836.

Burke EJ, Brown SJ. 2008. Evaluating Uncertainties in the Projection of Future Drought. *Journal of Hydrometeorology* **9**: 292–299, DOI: 10.1175/2007JHM929.1.

Bussay A, Szinell C, Szentimery T. 1999. *Investigations and measurements of droughts in Hungary*. Hungarian Meterological Service: Budapest.

Christensen JH, Christensen OB. 2007. A summary of the PRUDENCE model projections of changes in European climate by the end of this century. *Climatic Change* **81**: 7–30, DOI: 10.1007/s10584-006-9210-7.

Collins M. 2007. Ensembles and probabilities: a new era in the prediction of climate change. *Philosophical Transactions of the Royal Society* **365**: 1957–1970, DOI: 10.1098/rsta.2007.206.

Conover WJ, Johnson ME, Johnson MM. 1981. A comparative study of tests for homogeneity of variances, with applications to the outer continental shelf bidding data. *Technometrics* **23**: 351–361.

Crutcher HL. 1975. A note on the possible misuse of the Kolmogorov-Smirnov test. *Journal of Applied Meteorology* **14**: 1600–1603.

Dai A, Trenberth KE, Qian T. 2004. A global dataset of Palmer Drought Severity Index for 1870–2002: relationship with soil moisture and effects of surface warming. *Journal of Hydrometeorology* **5**: 1117–1130.

Déqué M, Rowell DP, Lüthi D, Giorgi F, Christensen JH, Rockel B, Jacob D, Kjellström E, de Castro M, van den Hurk B. 2007. An intercomparison of regional climate simulations for Europe: assessing uncertainties in model projections. *Climatic Change* **81**: 53–70, DOI: 10.1007/s10584-006-9228-x.

Déqué M, Somot S, Sanchez-Gomez E, Goodess CM, Jacob D, Lenderink G, Christensen OB. 2011. The spread amongst ENSEMBLES regional scenarios: regional climate models, driving general circulation Models and interannual variability. *Climate Dynamics* DOI: 10.1007/s00382-011-1053-x.

Dobler A, Ahrens B. 2008. Precipitation by a regional climate model and bias correction in Europe and South Asia. *Meteorologische Zeitschrift* **17**: 499–509.

Dubrovsky M, Svoboda MD, Trnka M, Hayes MJ, Wilhite DA, Zalud Z, Hlavinka P. 2008. Application of relative drought indices in assessing climate-change impacts on drought conditions in Czechia. *Theoretical and Applied Climatology* **96**: 155–171, DOI: 10.1007/s00704-008-0020-x.

FAO. 2003. *Digital Soil Map of the World and Derived Soil Properties cd-rom*. UNESCO: Rome.

Copyright © 2011 Royal Meteorological Society

Frei C, Christensen JH, Déqué M, Jacob D, Jones RG, Vidale PL. 2003. Daily precipitation statistics in regional climate models: Evaluation and intercomparison for the European Alps. *Journal of Geophysical Research* **108**(D3): 4124, DOI:10.1029/2002JD002287.

Giorgi F. 2006. Climate change Hot-Spots. *Geophysical Research Letters* **33**: L08707, DOI: 10.1029/2006GL025734.

Giorgi F, Coppola E. 2007. European climate-change oscillation (ECO). *Geophysical Research Letter* **34**: L21703, DOI: 10.1029/2007GL031223.

Giorgi F, Coppola E. 2009. Projections of 21st century climate over Europe. *European Physical Journal Conferences* **1**: 29–46, DOI: 10.1140/epjconf/e2009-00908-9.

Giorgi F, Mearns LO. 1991. Approaches to regional climate change simulation: A review. *Review of Geophysics* **29**: 191–216, DOI: 10.1029/90RG02636.

Giorgi F, Mearns LO. 1999. Introduction to special section: Regional climate modeling revisited. *Journal Geophysical Research* **104**: 6335–6352, DOI: 10.1029/98JD02072.

Gregory JM, Mitchell JFB, Brady AJ. 1997. Summer Drought in Northern Midlatitudes in a Time-Dependent CO2 Climate Experiment. *Journal of Climate* **10**: 662–686.

Guttman NB. 1999. Accepting the Standardized Precipitation Index: a calculation algorithm. *Journal of the American Water Resources Association* **35**: 311–322.

Hagemann S, Machenhauer B, Jones R, Christensen OB, Déqué M, Jacob D, Vidale PL. 2004. Evaluation of Water and Energy Budgets in Regional Climate Models Applied Over Europe. *Climate Dynamics* **23**: 547–567.

Hayes MJ, Svoboda MD, Wilhite DA, Vanyarkho OV. 1999. Monitoring the 1996 drought using the Standardized Precipitation Index. *Bulletin of the American Meteorological Society* **80**: 429–438.

Hayes MJ, Svoboda MD, Wall N, Widhalm M. 2010. The Lincoln declaration on drought indices: universal meteorological drought index recommended. *Bulletin of the American Meteorological Society*, DOI: 10.1175/2010BAMS3103.1.

Haylock MR, Hofstra N, Klein Tank AMG, Klok EJ, Jones PD, New M. 2008. A European daily high-resolution gridded dataset of surface temperature and precipitation. *Journal of Geophysical Research* **113**: D20119, DOI: 10.1029/2008JD10201.

Heddinghaus TR and Sabol P. A review of the Palmer Drought Severity Index and where do we go from here. *Preprints, Seventh Conf. on Applied Climatology* Dallas, TX, Amer. Meteor. Soc., 242–246.

Heim RR. 2002. A review of twentieth century drought indices used in the United States. *Bulletin of the American Meteorological Society* **83**: 1149–1165.

Hofstra N, Haylock M, New M, Jones PD. 2009. Testing E-OBS European high-resolution gridded dataset of daily precipitation and surface temperature. *Journal of Geophysical Research* **114**: D21101, DOI: 10.1029/2009JD011799.

Ji L, Peters AJ. 2003. Assessing vegetation response to drought in the northern Great Plains using vegetation and drought indices. *Remote Sensing of Environment* **87**: 85–98, DOI: 10.1016/S0034-4257(03)00174-3.

Keyantash J, Dracup JA. 2002. The Quantification of Drought: An Analysis of Drought Indices. *Bulletin of the American Meteorological Society* **83**: 1167–1180.

Labedzki L. 2007. Estimation of local drought frequency in central Poland using the standardized precipitation index SPI. *Irrigation and Drainage* **56**: 67–77, DOI: 10.1002/ird.285.

Lehner B, Döll P, Alcamo J, Henrichs T, Kaspar F. 2006. Estimating the Impact of Global Change on Flood and Drought Risks in Europe: A Continental, Integrated Analysis. *Climatic Change* **75**: 273–299, DOI: 10.1007/s10584-006-6338-4.

Lloyd-Hughes B, Saunders MA. 2002. A drought climatology for Europe. *International Journal of Climatology* **22**: 1571–1592, DOI: 10.1002/joc.846.

López-Moreno JI, Beniston M. 2009. Daily precipitation intensity projected for the 21st century: seasonal changes over the Pyrenees. *Theoretical and Applied Climatology* **95**: 375–384, DOI: 10.1007/s00704-008-0015-7.

McGregor JL. 1997. Regional climate modeling. *Meteorology and Atmospheric Physics* **63**: 105–117, DOI: 10.1007/BF01025367.

McKee TB, Doesken NJ, Kleist J. 1993. The relationship of drought frequency and duration to time scales. *Preprints of the 8th Conference on Applied Climatology*: 179–184.

Nakicenovic N, Alcamo J, Davis G, de Vries B, Fenhann J, Gaffin S, Gregory K, Grbler A, Jung TY, Kram T, La Rovere EL, Michaelis L, Mori S, Morita T, Pepper W, Pitcher H, Price L, Raihi K, Roehrl A, Rogner H-H, Sankovski A, Schlesinger M, Shukla P, Smith S, Swart R, van Rooijen S, Victor N, Dadi Z. 2000. *IPCC Special Report on Emissions Scenarios*. Cambridge University Press: Cambridge, United Kingdom and New York.

Palmer WC. 1965. *Meteorological drought*. U.S. Research Paper No. 45. US Weather Bureau: Washington, DC.

Piani C, Haerter JO, Coppola E. 2010. Statistical bias correction for daily precipitation in regional climate models over Europe. *Theoretical and Applied Climatology* **99**: 187–192, DOI: 10.1007/s00704-009-0134-9.

Räisänen J. 2002. CO2-Induced Changes in Interannual Temperature and Precipitation Variability in 19 CMIP2 Experiments. *Journal of Climate* **15**: 2395–2411.

Rowell PR. 2005. A scenario of European climate change for the late twenty-first century: seasonal means and interannual variability. *Climate Dynamics* **25**: 837–849, DOI: 10.1007/s00382-005-0068-6.

Rummukainen M. 2010. State-of-the-art-with regional climate models. *Wiley interdisciplinary reviews: Climate Change* **1**: 82–96, DOI: 10.1002/wcc.8.

Seiler RA, Hayes M, Bressan L. 2002. Using the standardized precipitation index for flood risk monitoring. *International Journal of Climatology* **22**: 1365–1376, DOI: 10.1002/joc.799.

Sheffield J, Wood EF. 2008. Projected changes in drought occurrence under future global warming from multi-model, multi-scenario, IPCC AR4 simulations. *Climate Dynamics* **31**: 79–105, DOI: 10.1007/s00382-007-0340-z.

Solomon S, Qin D, Maning M, Alley RB, Berntsen T, Bindoff NL, Chen Z, Chidtaisong A, Gregory JM, Hegerl GC, Heimann M, Hewitson B, Hoskins BJ, Joss F, Jouzel J, Kattsov V, Lohmann U, Matsuno T, Molina M, Nicholls N, Overpeck J, Raga G, Ramaswamy V, Ren J, Rusticucci M, Sommerville R, Stocker TF, Whetton P, Wood RA, Wratt D. 2007. In *Climate Change 2007: The Physical Science Basis. Contribution of Working Group I to the Fourth Assessment Report of the Intergovernmental Panel on Climate Change*, Solomon S, Qin D, Manning M, Chen Z, Marquis M, Averyt KB, Tignor M, Miller HL (eds). Technical Summary. Cambridge University Press: Cambridge, United Kingdom and New York, USA.

Suklitsch M, Gobiet A, Leuprecht A, Frei C. 2008. High Resolution Sensitivity Studies with the Regional Climate Model CCLM in the Alpine Region. *Meteorologische Zeitschrift* **17**: 467–476.

Suklitsch M, Gobiet A, Truhetz H, Awan NK, Göttel H, Jacob D. 2010. Error Characteristics of High Resolution Regional Climate Models over the Alpine Area. *Climate Dynamics* (in press). DOI: 10.1007/s00382-010-0848-5.

Szinell CS, Bussay A, Szentimrey T. 1998. Drought tendencies in Hungary. *International Journal of Climatology* **18**: 1479–1491.

Szalai S, Szinell C. 2000. Comparison of two drought indices for drought monitoring in Hungary – a case study: 161–166. In *Drought and drought mitigation in Europe*, Vogt JV, Somma F (eds). Kluwer: Dordrecht.

Themeßl MJ, Gobiet A, Leuprecht A. 2011. Empirical-statistical downscaling and error correction of daily precipitation from regional climate models. *International Journal of Climatology* **31**: 1530–1544, DOI: 10.1002/joc.2168.

Thornthwaite CW. 1948. An approach towards a rational classification of climate. *Geography Review* **38**: 55–94.

Trnka M, Dubrovsky M, Svoboda MD, Semeradova D, Hayes MJ, Zalud Z, Wilhite DA. 2008. Developing a regional drought climatology for the Czech Republic for 1961–2000. *International Journal of Climatology* **29**: 863–883, DOI: 10.1002/joc.1745.

van der Linden P, Mitchell JFB. 2009. *ENSEMBLES: Climate Change and its Impacts: Summary of research and results from the ENSEMBLES project*. Met Office Hadley Centre: Exeter.

van der Schrier G, Efthymiadis D, Briffa KR, Jones PD. 2007. European Alpine moisture variability for 1800–2003. *International Journal of Climatology* **27**: 415–427, DOI: 10.1002/joc.1411.

Vicente-Serrano SM, Beguería S, López-Moreno JI. 2010. A multiscalar drought index sensitive to global warming: The Standardized Precipitation Evapotranspiration Index – SPEI. *Journal of Climate* **23**: 1696–1718, DOI: 10.1175/2009JCLI2909.1.

Walter H, Lieth H. 1967. *Klimadiagramm-Weltatlas*. Gustav Fischer Verlag: Jena.

Wang Y, Leung LR, McGregor JL, Lee DK, Wang WC, Ding Y, Kimura F. 2004. Regional climate modeling: progress, challenges and prospects. *Journal of the Meteorological Society of Japan* **82**: 1599–1628.

Warren R, Yu R, Osborn T, de la Nava Santos S. 2009. Future European drought regimes under mitigated and un-mitigated climate

Copyright © 2011 Royal Meteorological Society

change. *IOP Conference Series: Earth and Environmental Science* **6**: 292012, DOI: 10.1088/1755-1307/6/9/292012.
Weber L, Nkemdirim L. 1998. Palmer's drought indices revisited. *Geografska Annaler* **80**: 153–172.
Wells N, Goddard S, Hayes MJ. 2004. A self-calibrating Palmer Drought Severity Index. *Journal of Climate* **17**: 2335–2351.
Wetherald RT, Manabe S. 1995. The mechanisms of summer dryness induced by greenhouse warming. *Journal of Climate* **8**: 3096–3108.
Wilhite DA. 1993. *Drought Assessment, Management and Planning: Theory and Case Studies*. Kluwer Academic Publishers: Boston, Dordrecht, London.
Wilhite DA, Glantz MH. 1985. Understanding the drought phenomenon: The role of definitions. *Water International* **10**: 111–120.
Wilks DS. 1995. *Statistical Methods in the Atmospheric Sciences*. Academic Press: London.
Wu H, Hayes MJ, Wilhite DA, Svoboda MD. 2005. The effect of the length of record on the standardized precipitation index calculation. *International Journal of Climatology* **25**: 505–520, DOI: 10.1002/joc.114.

Copyright © 2011 Royal Meteorological Society